Volume 12 | Number 24 | 21 December 2025

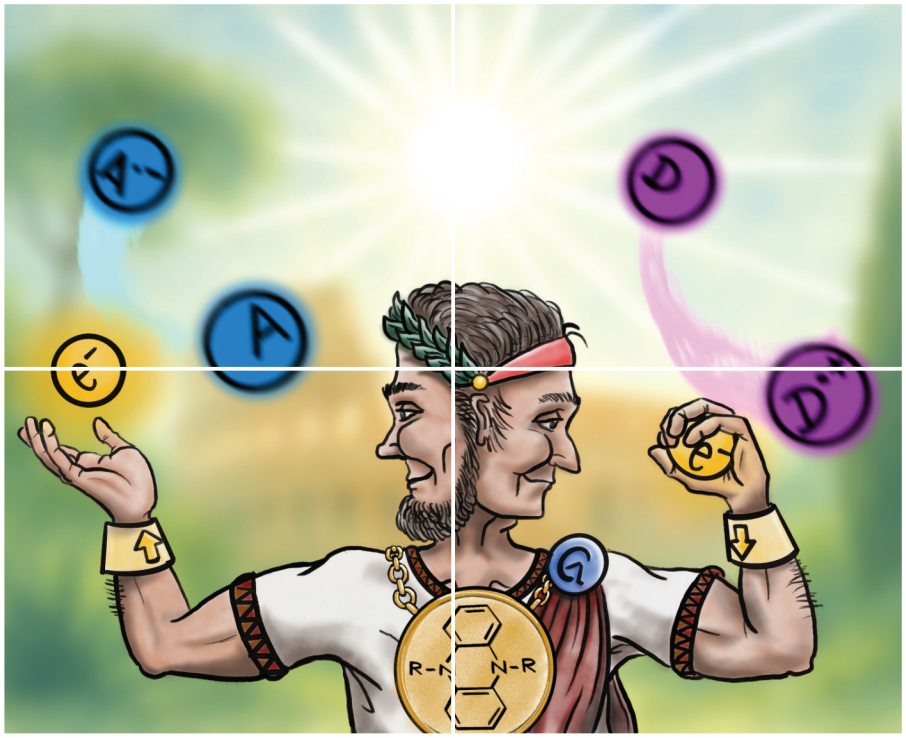

ORGANIC CHEMISTRY

FRONTIERS

CCS 中国化学会 CHINESE CHEMICAL SOCIETY
SIOC 1950
ROYAL SOCIETY OF CHEMISTRY
rsc.li/frontiers-organic

ORGANIC CHEMISTRY FRONTIERS

RESEARCH ARTICLE

View Article Online
View Journal | View Issue

Cite this: *Org. Chem. Front.*, 2025, **12**, 6798

Janus-type photo-redox properties and catalytic applications of 5,10-dihydrophenazine derivatives

Phung Phan Huyen Quyen,[a] Nina Hagmeyer,[b,c] Thanh Huyen Vuong,[a] Adrian Prudlik,[a] Robert Francke, [a] Benjamin Dietzek-Ivanšić†[b,c] and Esteban Mejía *[a,d]

Received 24th September 2025,
Accepted 7th November 2025

DOI: 10.1039/d5qo01348h

rsc.li/frontiers-organic

Inspired by the synthetic potential of organic photoredox catalysts, we synthesised and characterised a series of 5,10-dihydrophenazine derivatives that bear heterocycles as electron-withdrawing groups. Upon exploring their photocatalytic behaviour, we discovered that these compounds exhibit Janus-type reactivity, enabling both oxidative C(sp^3)–H cyanation and reductive aryl halide cleavage. We investigated their photophysical and electrochemical properties through cyclic voltammetry (CV), transient absorption spectroscopy (TA) and UV-Vis spectroelectrochemistry (SEC). Time-resolved UV-Vis spectroscopy and electron paramagnetic resonance (EPR) provided valuable information on excited-state dynamics and radical cation formation. This revealed that the catalysts act as effective reductants for C(sp^2)–I bond cleavage, generating aryl radicals. Furthermore, the excited-state radical cation facilitates the oxidative C(sp^3)–H cyanation of tertiary amines. Our mechanistic studies confirm the dual redox nature of these catalysts, thereby expanding the utility of 5,10-dihydrophenazine derivatives in photoredox catalysis.

Introduction

Catalysts play a crucial role in chemical reactions by providing efficient pathways that lower activation energy and enhance reaction kinetics, facilitating product formation. Consequently, the development of catalysts has become a major focus in chemistry.[1] Among the various types, photocatalysts have attracted considerable attention due to their unique reactivity, which enables the synthesis of complex organic molecules that would otherwise be unattainable.[2–4] In line with the growing demand for sustainable and green chemical processes, organic photoredox catalysts have emerged as viable alternatives to traditional metal-based systems. In line with the growing demand for sustainable and green chemical processes, organic photoredox catalysts have emerged as a viable alternative to traditional metal-based systems. Initially, research focused on using dyes as visible light-promoted catalysts in chemical transformations,[5] but the limited structural diversity of commercially available dyes necessitated the development of novel chromophore-based photocatalysts with broader applicability in various chemical processes.[6] To advance metal-free photoredox catalysis, reduced phenazines and their analogues with a 5,10-dihydrophenazine core have been introduced as efficient photocatalysts. One noteworthy approach to replacing traditional iridium (Ir)- or ruthenium (Ru)-based complexes involved using 5,10-dihydrophenazine derivatives as strong reducing agents, as demonstrated by Miyake *et al.* In their study, white light-emitting diode (LED) excitation facilitated the direct reduction of trifluoromethyl iodide (CF_3I), generating trifluoromethyl radicals that subsequently participated in substitution or addition reactions with unsaturated substrates.[7] Another innovative strategy by the same group used 5,10-dihydrophenazine derivatives in atom transfer radical polymerisation (ATRP•).[8,9] Their proposed mechanism suggested that the excited states of the catalyst participated in an oxidative quenching pathway with alkyl bromides, effectively minimising side reactions.[9,10] Based on literature examples, the activity can be summarised as shown in Fig. 1. The excited states of 5,10-dihydrophenazine derivatives can undergo photoinduced electron transfer (PET), which results in the one-electron reduction of substrates and the formation of radical cations (*i.e.* oxidative quenching). These radical cations can then regenerate their neutral ground states *via* electron transfer from donor molecules. Under certain conditions, 5,10-dihydrophenazine derivatives can undergo further oxidation to form

[a]*Leibniz Institute for Catalysis (LIKAT), Albert-Einstein-Str. 29a, 18059 Rostock, Germany. E-mail: Esteban.mejia@catalysis.de*
[b]*Institute of Physical Chemistry, Friedrich Schiller University Jena, Lessingstraße 4, 07743 Jena, Germany*
[c]*Leibniz Institute of Photonic Technology, Albert-Einstein-Straße 9, 07745 Jena, Germany*
[d]*Hanoi University of Science and Technology, 1 Dai Co Viet Road, Hanoi, Vietnam*
†Current address: Leibniz Institute of Surface Engineering, Permoserstraße 15, 04318 Leipzig, Germany

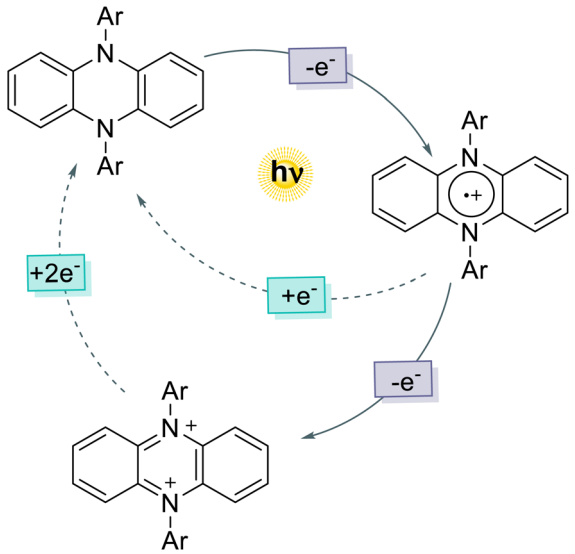

Fig. 1 General mechanism for oxidation of 5,10-dihydrophenazine derivatives (solid arrows) and reduction of cationic species (dashed arrows).

the highly reactive pyrazinium dication, which requires two electrons to return to its neutral ground state.

The PET step must be thermodynamically favorable, meaning that the redox potentials of the excited photocatalyst (PC*) and the substrate must be compatible. In particular, PC* can only reduce the substrate if the substrate's reduction potential (E_{red}) of is more positive than the oxidation potential (E_{ox}) of PC*.[11] Consequently, exciting PC with light increases its reducing power compared to the ground state.[12] The electronic state of PC* also influences its redox potential. In the triplet state (T_1), the contribution to the excited state energy is lower than in the singlet state (S_1). Consequently, S_1 relaxes to the ground state *via* fluorescence, whereas T_1 undergoes phosphorescence.[11,12] However, due to its longer lifetime, the T_1 state plays a crucial role in PET by increasing the probability of interaction between the substrate and PC*.[13] Furthermore, the intramolecular charge transfer character significantly extends the lifetime of the excited state, making it a key factor in the design of organic photoredox catalysts. Consequently, tuning the charge-transfer properties has become a major focus of catalyst structural modification.[14]

Several structural modifications to 5,10-dihydrophenazines have been introduced to take advantage of changes in photophysical properties, such as core extension and the incorporation of *N*-aryl substituents. Strategically altering the positions of these substituents results in observable changes in photophysical behaviour upon irradiation. Specifically, introducing *N*-aryl groups at nitrogen atoms or directly onto the core led to a red-shift in absorption due to stabilisation of the π* orbital by extended conjugation.[15] Extended-core *N*,*N*-diaryl-5,10-dihydrophenazines exhibited longer maximum absorption wavelengths compared to their non-extended counterparts. Additionally, significant differences in molar absorptivity ($\varepsilon_{max,abs}$) were noted between core-extended and non-core-extended derivatives. Interestingly, core-extended 5,10-dihydrophenazines substituted with electron-donating (OCH_3) or electron-withdrawing (CF_3) groups on the aryl ring showed only minor variations in absorption wavelength. This suggests that these substituents only slightly perturbed the electronic structure.[15]

Another intriguing feature of photocatalysts, beyond structural modification, is their ability to be tuned by external stimuli. For instance, the reduction potential of Rhodamine 6G (Rh-6G) varies depending on the redox state and the wavelength of the absorbed light. For instance, under visible-light irradiation, the reduction potential of Rh-6G*/Rh-6G$^{\bullet-}$ is approximately −0.8 V *vs.* SCE,[16] but shifts to approx. −1.0 V *vs.* SCE under green-light irradiation and to −2.4 V *vs.* SCE when irradiated with blue light.[16,17] Using this tunability, König *et al.* successfully employed blue-light irradiation to modulate the reduction potential of Rh-6G, enabling di-substituted C–H arylations using aryl bromides, a reaction that did not proceed under green-light irradiation.[16] Similarly, switching catalyst roles *via* multi-photon excitation has emerged as an effective method for oxidising substrates with highly positive oxidation potentials. For instance, Wickens *et al.* showed that the excited-state *N*-phenylphenothiazine (PTH) radical cation (formed by photooxidation) acts as a powerful oxidising agent, capable of oxidising benzene (E_{ox} = +2.5 V *vs.* SCE) and various benzene derivatives, including toluene, *m*-xylene, and mesitylene.[18] Achieving these potentials with conventional photocatalysts is very challenging and requires high-energy illumination.[19]

Inspired by these developments and the use of excited 5,10-dihydrophenazines in ATRP,[9] as well as our own experience of using 5,10-dihydrophenazine radical cations as catalysts under thermal conditions (both in homogeneous and heterogeneous systems),[20–22] we hypothesised that both the neutral and the radical cation excited states of 5,10-dihydrophenazines could function as a photoredox catalyst (PC, Fig. 2). Upon absorving a photon, the excited state can exhibit Janus-type reactivity, acting as either a strong reductant (path 1, where A serves as the electron acceptor), or a strong oxidant. The resulting open-shell species can undergo further photoexcitation, followed by electron transfer with an organic substrate, ultimately regenerating the catalyst (path 2, where D serves as the electron donor).

Results and discussion

Catalyst synthesis

Although studies have explored 5,10-dihydrophenazine derivatives with common electron-withdrawing groups (CF_3, CN) *via* *N*-aryl substitution,[9,20] the incorporation of electron-withdrawing heterocycles into the 5,10-dihydrophenazine core remains unexplored. Pyridine and pyrimidine are electron-poor heterocycles, meaning their electron density is lower than that of typical aromatic rings, resulting in inherent π-deficiency. In

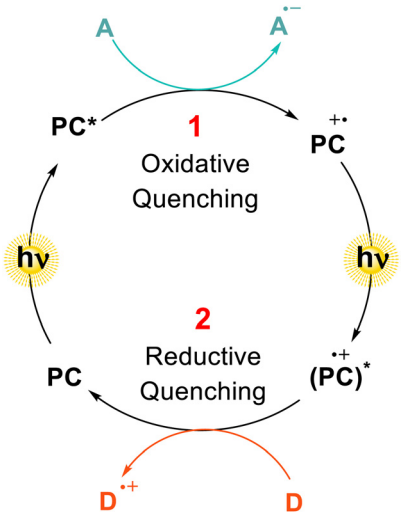

Fig. 2 The Janus-type reactivity of the 5,10-dihydrophenazine-derived photocatalyst (PC): when a photon is absorbed, the excited state (PC*) acts as a strong reductant (path 1), with A serving as the electron acceptor. The resulting open-shell species can undergo further photoexcitation, becoming a strong oxidizing agent that can accept an electron from a donor (D, path 2), ultimately regenerating the catalyst.

view of this interesting property, we sought to incorporate these heterocycles into the 5,10-dihydrophenazine framework as an alternative to conventional electron-withdrawing groups. We employed the Buchwald–Hartwig cross-coupling reaction for the synthesis of these compounds, following a previously reported procedure (see Table 1).[9] In our case, this method proved effective for synthesising of 5,10-dihydrophenazine derivatives bearing 2- or 3-bromopyridine. Specifically, introducing of 2-bromopyridine produced compound **1a** with an 89% yield, whereas using 3-bromopyridine produced compound **1b** in 60% yield. In contrast, applying this strategy to pyrimidine derivatives was less effective, highlighting the limitations of the cross-coupling approach for these substrates.

The yield of cross-coupling products decreased as the nitrogen content of aromatic heterocycles increased. Transitioning from pyridine to pyrimidine derivatives resulted in greater π-deficiency, which may have hindered the C–N cross-coupling reaction. For instance, using 5-bromopyrimidine instead of 2-bromopyridine to synthesise compound **1c** resulted in a significantly lower yield of 7%. Additionally, the position of the nitrogen atoms affected the success of cross-coupling with the reduced phenazine core. Specifically, 2-bromopyrimidine yielded the monosubstituted product **1g** more efficiently than the disubstituted product **1h**, whereas 5-bromopyrimidine favoured the formation of the disubstituted product **1c**. Furthermore, the cross-coupling reaction between 2-bromopyrimidine and 5,10-dihydrophenazine exhibited reduced efficiency. The twofold cross-coupling product **1h** (see Fig. 3 and Fig. S6) formed in a yield of less than 5%, while the mono C–N coupling product **1g** was obtained in a yield of 32%. Attempts to synthesise **1h** from **1g** or to improve the yield of **1c** were unsuccessful, as **1h** appears unstable under the selected reaction conditions. This was confirmed by the isolation of the corresponding decomposition product, **1i**, which was formed by the ring opening of **1h** *via* a 1,3-N sigmatropic shift (see the single crystal X-ray structure in Fig. S7). To compare the photophysical and electrochemical properties with those of the other compounds, we synthesised **1d** and **1f**, incorporating an electron-donating tolyl group and a π-delocalised system (2-naphthyl), yielding 50% and 51%, respectively. Additionally, we included the commercially available compound **1e** in our study for reference. Finally, we anticipated that these cross-coupling products might exhibit similar properties to 5,10-dihydrophenazine analogues bearing CF_3 or CN substituents, where π* orbital stabilisation is enhanced through delocalisation on the phenyl rings rather than the 5,10-dihydrophenazine core.[9]

Interestingly, most 5,10-dihydrophenazine derivatives are typically found to adopt an almost planar conformation, with the aromatic groups at positions 5 and 10 oriented almost perpendicular to the phenazine backbone.[23] In contrast, compound 1H displays a pronounced saddle-shaped distortion, which is likely to be caused by the effect of the nitrogen atoms in the *ortho* positions of the heteroaromatic rings (Fig. 3).

Photophysical and electrochemical studies

Absorption spectra were recorded for these compounds to evaluate their light-absorbing capabilities (see Fig. 4A). Overall, the compounds showed absorption in the near-UV region. Compounds **1a–c** exhibited absorption maxima ranging from 310 to 365 nm, whereas compounds **1d** and **1f** showed notable red-shifted absorption. Compound **1c** is particularly expected to exhibit an increased contribution from n,π* excitation compared to compounds **1a–b**, resulting in a wavelength shift. However, introducing additional π-conjugation in compounds **1a–b** did not increase their absorption maxima compared to compound **1e**, which lacks such conjugation. Similarly, no clear correlation was found between electron-donating substituents or extended conjugation systems and the light-absorbing properties of compounds **1d** and **1f**. In contrast, radical cations ($\mathbf{1}^{\bullet+}$) and dications ($\mathbf{1}^{2+}$) exhibited significantly red-shifted absorption extending into the visible range, in contrast to their neutral analogues (see below). This observation highlights the potential of using radical cations (or dications) as effective photocatalysts due to their broader visible-light absorption.

The CV results demonstrate that compounds **1a–g** undergo chemically reversible oxidation processes, characterised by two distinct and well-defined redox couples resulting from two consecutive single-electron oxidation events (see SI, Section 10). This chemical reversibility indicates a relatively high stability of the radical cations and dications, which is a basic requirement for use in photocatalysis. The ground-state oxidation potentials for the first oxidation step ($\mathbf{1}/\mathbf{1}^{\bullet+}$) ranged from +0.14 to +0.33 V *vs.* SCE, whereas the second oxidation step ($\mathbf{1}^{\bullet+}/\mathbf{1}^{2+}$) occurred between +0.56 and +1.09 V *vs.* SCE (see Table 2).

Table 1 Preparation of 5,10-dihydrophenazine derivatives *via* Pd-catalyzed Buchwald–Hartwig cross-coupling[a,b]

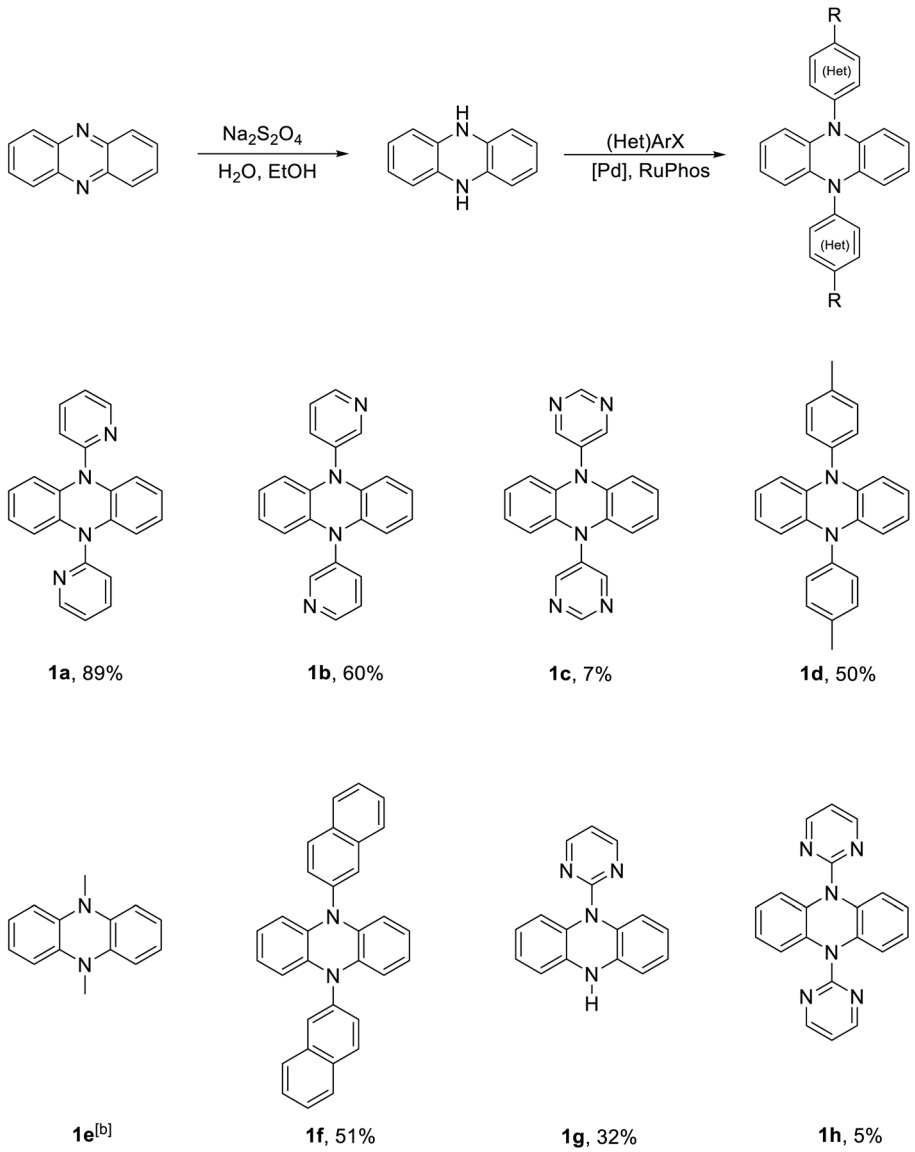

[a] General reaction conditions: 5,10-dihydrophenazine (1.2 mmol, 1.0 eq.), RuPhos (0.044 mmol, 4 mol%), RuPhos precatalyst (0.043 mmol, 4 mol%), NaO*t*Bu (4.5 mmol, 4.0 eq.), (het)aryl halide (4.5 mmol, 4.0 eq.), in THF or 1,4-dioxane, stirred at reflux temperature for up to 48 h. Complete experimental details for each product including isolated yields can be found in the SI. [b] Obtained from commercial sources.

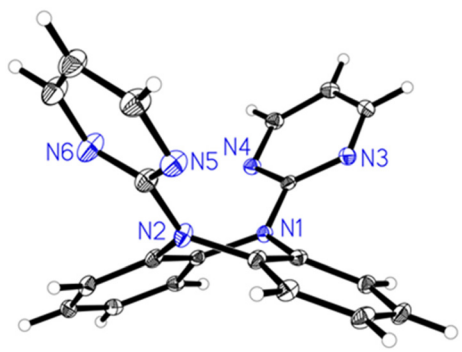

Fig. 3 Single crystal X-ray Molecular structure of **1h**. Displacement ellipsoids correspond to 30% probability.

The photophysical properties of the radical cations and dications derived from the selected compounds **1a**, **1d**, **1e** and **1f** (which exhibited greater stability and could be synthesised in larger quantities) were investigated using UV-Vis spectroelectrochemistry (SEC) at potentials close to $E_{ox}(\mathbf{1})$. This determined their absorption maxima within the visible spectrum. Fig. 4B shows the absorption spectra of the pure components of the radical cations ($\mathbf{1}^{\bullet+}$), highlighting their red-shifted absorption extending into the visible range, particularly within the red spectral region.[24] These radical cations generally displayed weak, low-intensity absorption in the UV range, but exhibited characteristic absorption profiles in the visible region, showing distinct maxima in both the blue and red

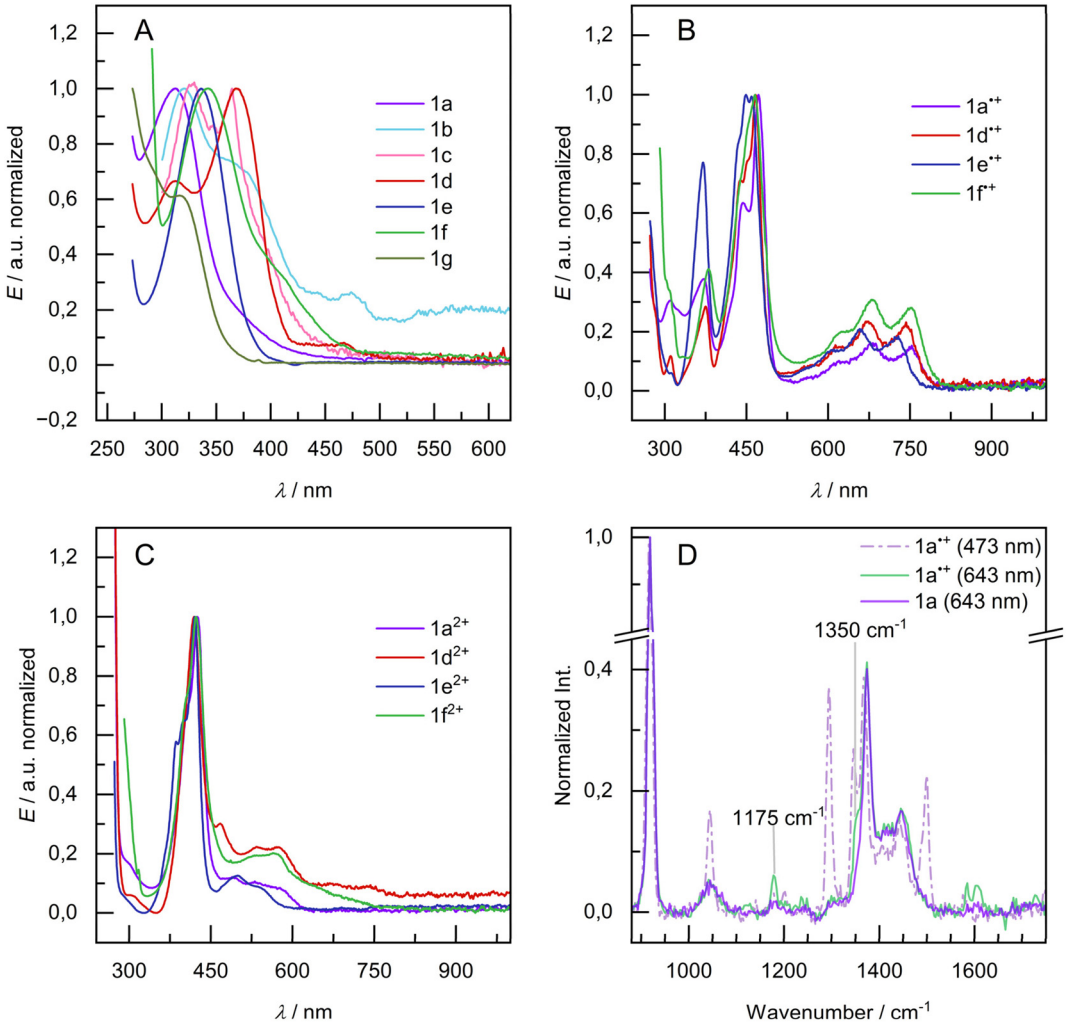

Fig. 4 Normalized UV-Vis absorption spectra of 5,10-dihydrophenazine derivatives measured in MeCN (**1a–e**, **1g**) and in THF (**1f**) in their neutral state (A), as well as pure component spectra obtained from UV-Vis SEC data for selected electro-generated radical cations (B) and dications (C). Resonance Raman spectra of $\mathbf{1a}^{\bullet+}$ in MeCN upon excitation at 473 nm (purple line, dashed-dotted) and 643 nm (green line), as well as of **1a** upon excitation at 643 nm (purple line) (D). UV-Vis and rR SEC were carried out in acetonitrile (0.1 M Bu_4NPF_6/CH_3CN) except for **1f** (for details, see the SI).

regions. Specifically, radical cation $\mathbf{1a}^{\bullet+}$ exhibited strong absorption peaks at 472 nm (blue region) and at 684 nm and 753 nm (red region). Other radical cations showed similar absorption maxima in the blue region, ranging from 457 to 468 nm, and in the red region, ranging from 659 to 754 nm. These findings highlight their potential as open-shell photocatalysts operating within the visible region.

Fig. 4C shows the absorption spectra of the dications ($\mathbf{1}^{2+}$). These dications generally exhibited maximum absorption wavelengths at approximately 430 nm, with no observable absorption in the red region. The absence of absorption in the red region likely results from the loss of two electrons from the nitrogen atoms within the 5,10-dihydrophenazine core, which prevents n–π* transitions.

We performed resonance Raman (rR) spectroelectrochemistry further to characterise the Franck–Condon states of the radical cations $\mathbf{1a}^{\bullet+}$, $\mathbf{1d}^{\bullet+}$ and $\mathbf{1f}^{\bullet+}$ upon excitation at 473 and 643 nm. Upon oxidation and excitation at 473 nm, all of the three compounds show peaks around 1290 cm^{-1}, 1345 cm^{-1}, and 1490–1500 cm^{-1} (see Fig. 4D and Fig. S25A–C). Based on literature,[25] these bands are associated with the C–C stretching vibrations localised on the dihydrophenazine core. Another oxidation-induced band at 1040 cm^{-1} is observed for $\mathbf{1a}^{\bullet+}$ and $\mathbf{1d}^{\bullet+}$. It is associated with a C–N stretching and C–H in-plane bending mode.[25] Such a vibrational band may also be present in $\mathbf{1f}^{\bullet+}$ as well, as deduced from the slight increase in signal intensity at around 1024 cm^{-1} (Fig. S25C). However, the strong solvent peak prohibits definitive conclusions. A band unique to $\mathbf{1a}^{\bullet+}$ evolves at 1203 cm^{-1}.

Upon excitation at 643 nm, peaks at 1175 cm^{-1} and 1350 cm^{-1} dominate the spectra, with new bands evolving around 1600 cm^{-1} due to ring C–C stretching (see Fig. 4D and Fig. S25D–F). Some of the peaks observed at 473 nm remain visible, albeit at much lower intensity. The data suggest that

Table 2 UV-Vis absorption maxima and redox potentials at ground and excited states of compounds **1a–1g**

	1a	1b	1c	1d	1e	1f	1g
$\lambda_{max,\ abs}$ (**1**) (nm)	310	320	365	370	336	341	—
$\lambda_{max,\ abs}$ ($\mathbf{1}^{\bullet+}$) (nm)	472	—	—	466	450	465	387
$\lambda_{max,\ abs}$ ($\mathbf{1}^{2+}$) (nm)	425	—	—	419	419	423	463
$E(\mathbf{1}/\mathbf{1}^{\bullet+})$ (V *vs.* SCE)	0.32	0.30	—	0.16	0.14	0.33	0.33
$E(\mathbf{1}^{\bullet+}/\mathbf{1}^{2+})$ (V *vs.* SCE)	1.08	1.09	—	0.98	0.94	0.95	0.56
$E(\mathbf{1}^{\bullet+}/\mathbf{1}^{\bullet+})$ (V *vs.* SCE)	−2.38[a]	—	—	−2.81[b]	−2.93[c]	−2.36[a]	—
$E([\mathbf{1}^{\bullet+}]^*/\mathbf{1})$[d] (V *vs.* SCE)	+2.03 (+1.65)[e]	—	—	+1.84[e]	—	+1.65[e]	—

[a] Excited wavelength for emission at 340 nm. [b] Excited wavelength for emission at 350 nm. [c] Excited wavelength for emission at 360 nm. [d] Excited wavelength for emission at 473 nm. [e] Excited wavelength for emission at 643 nm.

both excitation wavelengths result in optical transitions associated with the 5,10-dihydrophenazine core. This reflects the fact that the absorption spectra of the radical cations are not significantly affected by the substituent. However, the spectral patterns observed at 643 nm differ from those recorded at 473 nm. This indicates that the Franck–Condon points for the different wavelengths are distinct, *i.e.* different excited states are populated when the wavelength of excitation is shifted across the absorption band. This conclusion is consistent with quantum chemical calculations on related 5,10-dihydrophenazines, which predict an $S_1 \leftarrow S_0$ transition upon excitation at 643 nm, with population of a higher-lying S_n state with higher energy excitation.[26]

Although the excited-state redox potentials ($E(\mathbf{1}/\mathbf{1}^{\bullet+})$) cannot be directly measured by cyclic voltammetry (CV), they can be estimated by combining ground-state oxidation potentials with the corresponding excited-state energies ($\varepsilon_{0,0}$). The latter are determined from the Stokes shift, which is calculated as the difference between the absorption and emission maxima (see SI for details).[11] Using this approach, the excited-state oxidation potentials of compounds **1a**, **1d**, **1e**, and **1f** were estimated to range from −2.36 to −2.93 V *vs.* SCE (see Table 2), indicating that these excited states are strong reductants. These values are significantly influenced by substituents: compounds **1a** and **1f**, which bear electron-deficient groups or extended π-conjugation, are slightly weaker reductants compared to **1d** and **1e**, which incorporate electron-donating groups. A similar trend has been reported for *N*,*N*-diphenyl-5,10-dihydrophenazine derivatives bearing methoxy (OMe), trifluoromethyl (CF_3), or cyano (CN) substituents.[9] Moreover, the excited-state redox potentials of these compounds are higher than those of traditional metal-based photocatalysts such as $[Ru(bpy)_3]^{2+}$ ($E^*_{ox} = -0.81$ V *vs.* SCE) and $Ir(ppy)_3$ ($E^*_{ox} = -1.73$ V *vs.* SCE),[27] highlighting highlighting their superior reducing power in the photoexcited state.

Additionally, the excited-state redox potentials of radical cations $[\mathbf{1}^{\bullet+}]^*$ were also investigated. Using the Stokes shift (calculated as the difference between the absorption and emission maxima; see SI for details),[11] the excited-state redox potentials ($[\mathbf{1}^{\bullet+}]^*/\mathbf{1}$) were estimated to range from 1.65 to 2.03 V *vs.* SCE (Table 2). These values highlight the significant capabilities of excited radical cations as strong oxidants in chemical transformations.

As mentioned above, *N*-aryl substitution causes a change in the photophysical properties of 5,10-dihydrophenazine compounds. More specifically, the lowest excited state in derivatives with electron-donating groups is a locally excited (LE) state. Conversely, *N*-aryl substituents with an electron-withdrawing effect or extended π-conjugation result in a lowest-energy excited state with charge-transfer (CT) character. In order to gain insight into photoinduced excited-state dynamics and learn about the role of the pyridine substituent as an alternative to conventional electron-withdrawing groups, femtosecond transient absorption (fs-TA) spectroscopy was performed on **1a** and **1d–f** in acetonitrile (MeCN) and *N*,*N*-dimethylformamide (DMF). For **1f**, tetrahydrofurane (THF) was used instead of MeCN due to the molecule's poor solubility in the latter. The following discussion will focus primarily on the DMF measurements, which were used in the dehalogenation reaction to be discussed later. Immediately after photoexcitation, **1d** exhibits excited-state absorption (ESA) consisting of a double peak between 400 and 480 nm, as well as a featureless band between 500 and 670 nm which increases towards longer wavelengths (see Fig. 5A). Within 8 ns of excitation, the 450 nm band increases, while the 420 nm band and the feature in the red spectral region decrease. This general spectral shape is very similar to that reported for *N*,*N*-diphenyl-5,10-dihydrophenazine and other analogues with electron-donating substituents.[28,29] These electron-rich *N*,*N*-diphenyl-5,10-dihydrophenazines usually possess S_1/T_1 states of LE character, *i.e.*, electron density changes upon optical excitation are localized on the phenazine core.[10,28] Considering the spectral similarity, as well as the relatively electron-donating effect of the tolyl substituent, we also attribute the spectral features of **1d** to LE states. For further analysis, a global triexponential fit was applied to the data.

The fit yielded characteristic time constants of τ_1 = 5 ps, τ_2 = 88 ps, as well as a long τ_3, which lies beyond the range accessible by our setup. The first process reflects internal conversion (IC) from a higher-lying singlet state to the lowest excited and emissive singlet state and the timescale determined experimentally agrees with reports in the literature for IC of similar derivatives.[28] This interpretation is further supported by the decrease in the TA signal between 450 and 580 nm, which accompanies the process and coincides with the steady-state emission of the compound (see Fig. S24).

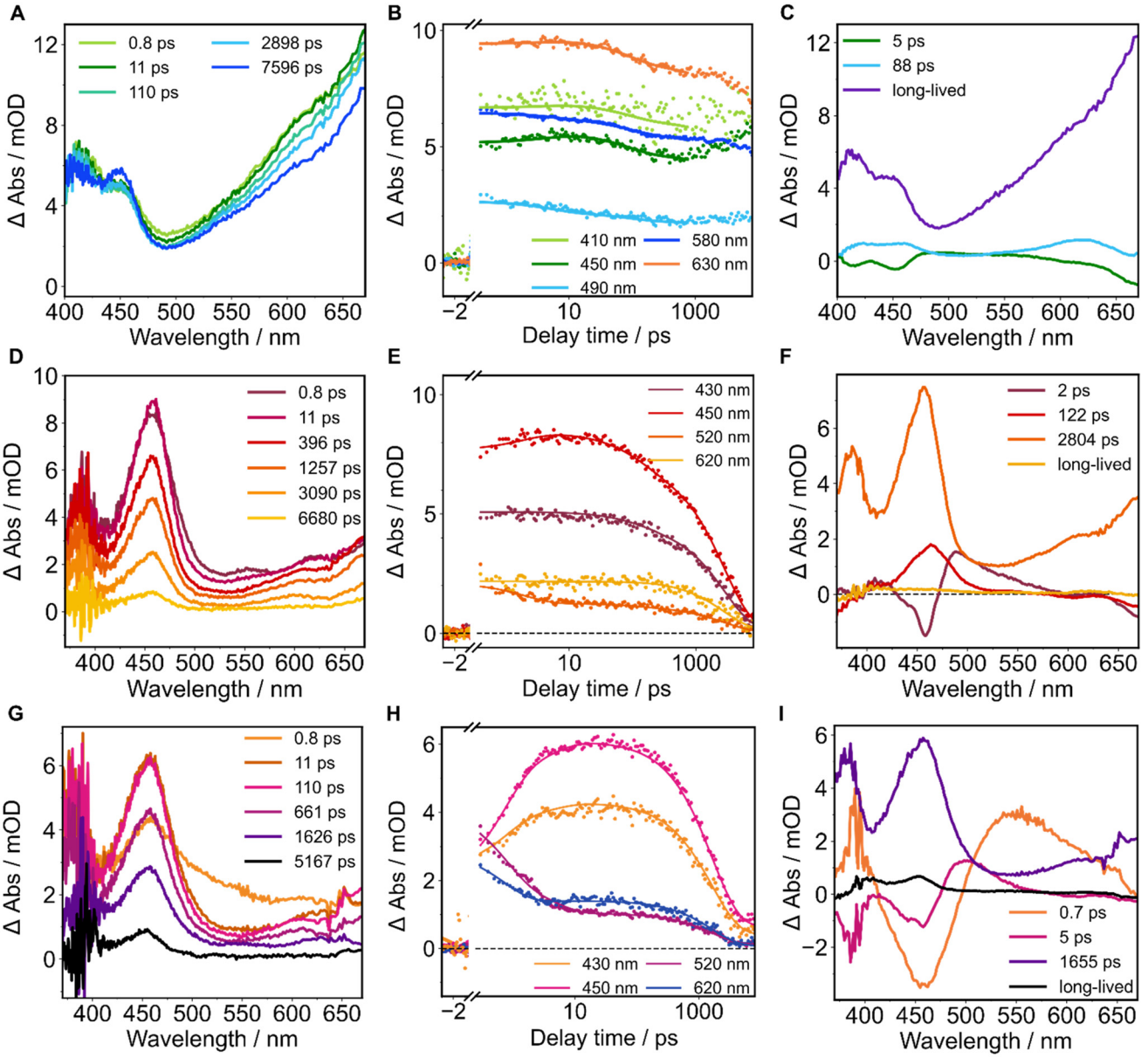

Fig. 5 Transient absorption spectra of **1d** in DMF at selected delay times after excitation (A), kinetic traces at selected wavelengths (B) and corresponding DAS (C) obtained from global analysis. Transient absorption spectra of **1f** in DMF at selected delay times after excitation (D), kinetic traces at selected wavelengths (E) and corresponding DAS (F) obtained from global analysis. Transient absorption spectra of **1a** in DMF at selected delay times after excitation (G), kinetic traces at selected wavelengths (H) and corresponding DAS (I) obtained from global analysis.

Therefore, the spectral change can be understood as an increase in emission from the S_1 state. The second process (τ_2), which takes place on a similar timescale to that reported for vibrational cooling in the S_1 state of other *N*,*N*-diphenyl-5,10-dihydrophenazine derivatives,[28] was observed to accelerate in MeCN (~35 ps, see Fig. S26). As DMF and MeCN have similar polarities, this difference is probably due to the higher viscosity of DMF (η = 0.92 mPa·s) compared to MeCN (η = 0.35 mPa·s). The results suggest a structural change associated with the vibrational relaxation of the excited molecule. The literature reports that the bending angle of the phenazine core is reduced in the excited state,[30] which may represent the intramolecular motion associated with τ_2. This flattening would also affect the position and geometry of the substituents relative to the phenazine core (bending motion and/or rotation; see Fig. 6). This internal structural change is slowed in the more viscous DMF.

On a nanosecond timescale, an increase in the 455 nm band at is observed while the other spectral features decrease. As previously mentioned, this spectral change is not accurately reflected in the fit and is most clearly visible in the TA spectra (Fig. 5A and B). The signal at 455 nm is characteristic of the triplet state of phenazine derivatives,[29,31,32] so we attribute the spectral change to intersystem crossing (ISC).

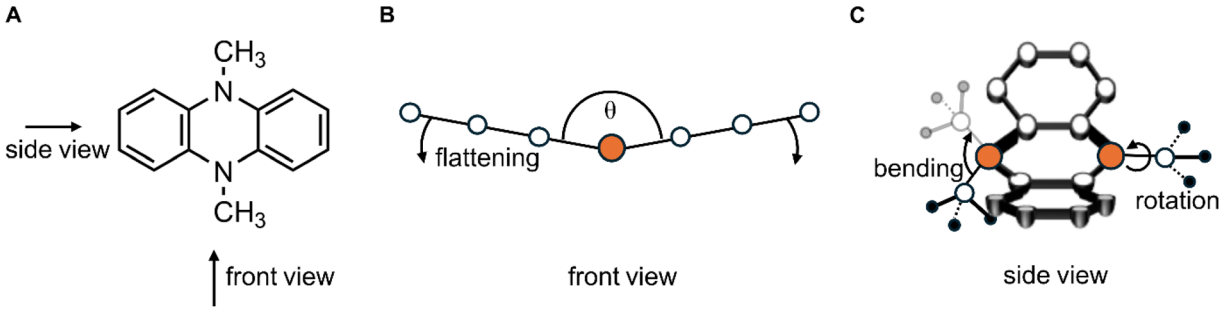

Fig. 6 Schematic representation of the flattening of 1e (A) in the excited state (B) and the simultaneous bending/rotation of the substituent (C).

The TA spectra for **1a** (electron-withdrawing substituent) and **1f** (extended π-system) are dominated by a band around 455 nm (see Fig. 5D and G). Additionally, a broad absorption feature increases towards longer wavelengths above 500 nm and shows a weak shoulder at around 605 nm. This spectral shape is similar to that of the radical cation (see Fig. 4D and Fig. S26), where the positive charge is primarily located on the phenazine core. This indicates that a CT state is formed upon optical excitation, whereby charge is transferred from the phenazine core to one or both N-substituents. These results are consistent with those reported for 5,10-dihydrophenazines with electron-withdrawing or π-extended aryl substituents.[10,28,33] The faster overall decay of the transient absorption features compared to **1d**—the decrease in differential absorbance to below 50% occurs within 1.6 ns (compared to ESA intensity at 10 ps)—is explained by stronger CT state stabilisation in polar solvents. This results in a smaller energy gap between the S_1 and S_0 states, leading to faster non-radiative decay in accordance with the energy gap law. This behaviour has also been reported for other *N*,*N*-disubstituted 5,10-dihydrophenazines when the substituents are changed from electron-donating to electron-accepting groups.[10,28,34] In DMF, the datasets of both compounds are best fitted by a sum of four exponentials.

For **1f**, the corresponding characteristic time constants are τ_1 = 2 ps, τ_2 = 122 ps and τ_3 = 2.8 ns while the fourth process takes place on a timescale beyond the dynamic range accessible by our setup. Despite the CT character of the excited states of **1f**, the processes associated to τ_1 and τ_2 seem to be identical to the ones observed in **1d**. As previously discussed, we attribute these processes to IC in conjunction with solvent reorganization (τ_1) and (structural) relaxation within the S_1 state (τ_2). The hypsochromic shift of the ESA band associated with τ_1 (see the corresponding decay-associated spectrum in Fig. 5F) is consistent with IC and solvent reorganization. The process associated with τ_2 shows the same solvent dependence as that observed for **1d**, *i.e.*, the process is slowed down in the more viscous DMF compared to THF (τ_2 = 55 ps, see Fig. S26D–F). Again, this behaviour suggests structural reorganization, although the smaller polarity of THF may also affect the excited-state dynamics. The characteristic time constant τ_3 is similar to the lifetime of the S_1 state of **1f** in dimethylacetamide (DMAc).[33] Considering the similar dielectric constants of DMAc (ε = 37.8) and DMF (ε = 36.7), it is reasonable to assume that the S_1 lifetime does not change drastically in the latter. We therefore attribute τ_3 to the depopulation of the S_1 state (and the formation of the triplet state). This is reflected in the peak at 455 nm, which persists at delay times beyond 5 ns (see Fig. 5D and F). The triplet state decays with a time constant (τ_4), which exceeds the dynamic range of our experiment by far. The given interpretation is supported by the fit of the data measured in THF (see Fig. S26D–F), which does not yield a component of ~3 ns. According to the energy gap law, the depopulation of the S_1 state is slowed down due to the less stable CT state in the less polar THF.

For **1a**, global analysis yields the characteristic time constants τ_1 = 0.7 ps, τ_2 = 5 ps and τ_3 = 1.6 ns in addition to a long-lived component. In line with the arguments presented above for **1d** and **1f**, τ_1 is assigned to IC and solvent reorganization and τ_3 is interpreted as ISC from the S_1 state to a long-lived triplet state. A significant difference between **1a** and **1f** is the process associated with τ_2, which proceeds one order of magnitude faster (τ_2 = 5 ps in DMF, τ_2 = 5 ps in MeCN) and is not affected by the solvent (see Fig. 5G–I and Fig. S26G–I). It is hypothesised that an H-bond forms between the nitrogen of the pyridyl substituent of **1a** and a hydrogen atom of the outer ring of the phenazine core. This hydrogen bond hinders the structural change observed in the other two compounds and results in less geometric rearrangement in the excited state. Consequently, the process is much faster in **1a** and not slowed down by a higher solvent viscosity. As with **1d** and **1f**, the 455 nm band of the long-lived species is indicative of the triplet state so that τ_3 describes the depopulation of S_1 by radiative and non-radiative decay to S_0 as well as by ISC.

In addition to the neutral compounds, we investigated the excited-state dynamics of the radical cations $\mathbf{1a}^{\bullet+}$, $\mathbf{1d}^{\bullet+}$, $\mathbf{1e}^{\bullet+}$ and $\mathbf{1f}^{\bullet+}$, which play an integral role in the photocatalytic cycle. Femtosecond transient absorption spectroelectrochemistry (TA-SEC) was performed upon excitation at two different wavelengths (*i.e.*, 460 and 680 nm) to investigate the photophysics of the cations.

The general shape of the TA spectra is very similar across the different compounds. They are dominated by an ESA below 420 nm, a GSB between 420 and 490 nm and an ESA between

500 and 580 nm. Another GSB region is observed above 580 nm, but the low oscillator strength of the transition(s) and the limited signal-to-noise ratio mean that the latter do not contribute significantly to the experimental data. Comparing the spectra after excitation at 460 and 680 nm reveals differences in the band ratios and spectral evolution for all compounds.

For **1a**$^{\bullet+}$ (see Fig. 7), the ESA maximum around 500 nm shifts dynamically to shorter wavelengths by 15 nm (*i.e.* 0.08 eV) within the first 40 ps after excitation at 460 nm. Moreover, the band around 380 nm decreases so that the peak ratio of the bands at 380 and 500 nm (*i.e.* $A_{380}:A_{500}$) decreases from 12.5 after 5 ps to ~5.7 after 55 ps. After excitation at 680 nm, the blueshift of the maximum around 500 nm is less pronounced (5 nm; 0.03 eV) and the change in the ratio of the peak intensities at 380 nm and 500 nm ($A_{380}:A_{500}$) is smaller (~4.9 at 5 ps and 5.4 at 57 ps after excitation). This indicates that **1a**$^{\bullet+}$ undergoes excitation wavelength-dependent relaxation pathways.

Global analysis of the excitation wavelength-dependent data also reflects these relaxation pathways. Upon excitation at 680 nm, only two characteristic time constants are required to appropriately describe the data: $\tau_{1,r}$ = 18 ps and $\tau_{2,r}$ = 62 ps. However, the data recorded upon excitation at 460 nm require an additional component yielding $\tau_{1,b}$ = 4 ps, $\tau_{2,b}$ = 19 ps and $\tau_{3,b}$ = 56 ps. The characteristic time constants of the slowest process in each dataset as well as the spectral shapes of the corresponding DAS match so that, regardless of the excitation wavelength, they are assigned to the same process. This process is characterised by a concomitant decay of the ESA bands and the GSB and, therefore, ascribed to ground-state relaxation from the D_1 state (see Fig. 8A). For 680 nm excitation, τ_1 reflects the vibrational relaxation within the D_1 state. The assignment is based on DFT calculations on similar derivatives,[26] which predict population of the lowest excited state (D_1) upon excitation at 680 nm, as well as on the DAS, which does not exhibit GSB decay. The latter indicates that relaxation in the excited state is occurring.

Although the process described by $\tau_{2,b}$ proceeds with a similar characteristic time constant, *i.e.*, $\tau_{2,b}$ = 19 ps compared to $\tau_{1,r}$ = 18 ps, it is accompanied by different spectral changes (see Fig. 7). Therefore, $\tau_{2,b}$ is not assigned to relaxation within the D_1 state. It can be concluded that $\tau_{1,b}$ and $\tau_{2,b}$ describe processes that are not initiated by 680 nm excitation. While absorption of red light directly populates the D_1 state, absorption of blue light populates higher-lying D_N states. This is reflected in our rR-SEC measurements, which show excitation wavelength-dependent rR features. Based on that and the

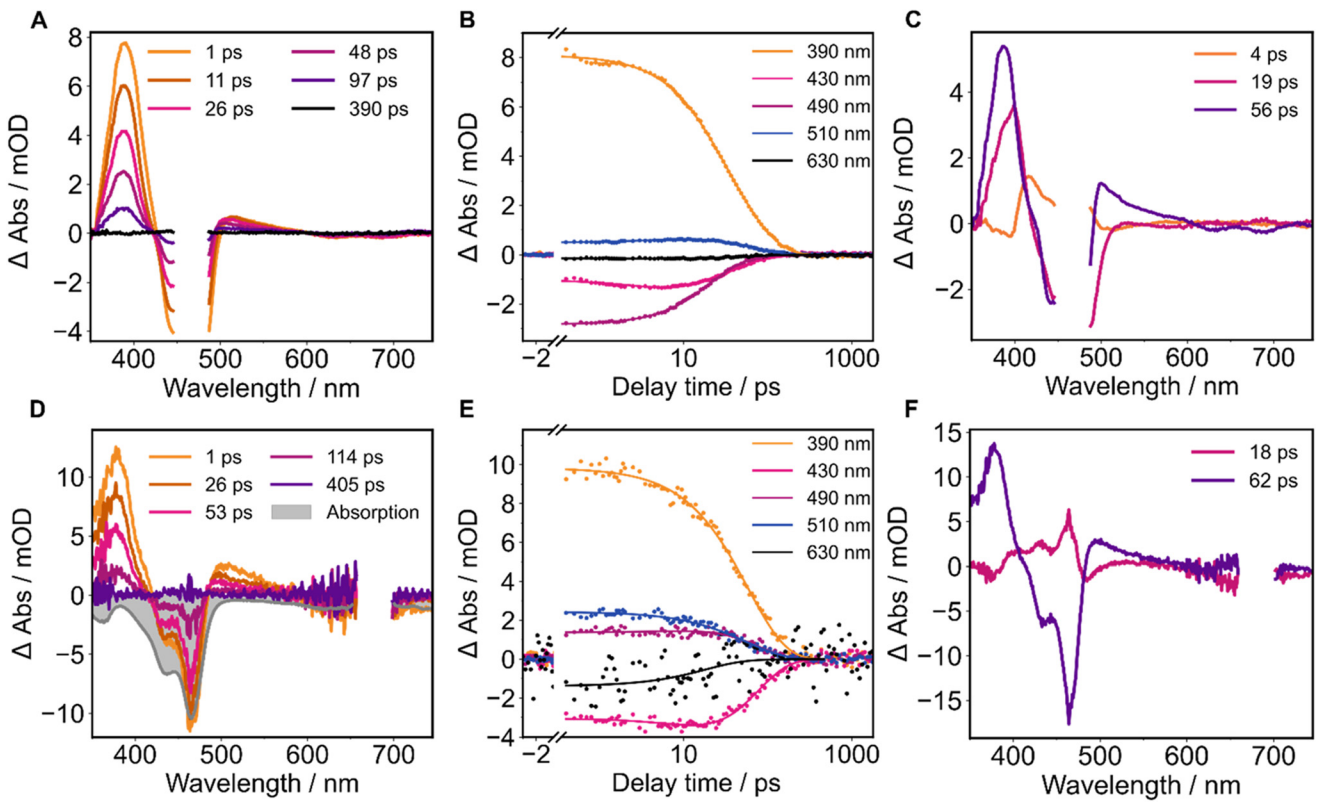

Fig. 7 Transient absorption spectra of **1a**$^{\bullet+}$ in MeCN obtained *via* TA-SEC at selected delay times after excitation at 460 nm (A), kinetic traces at selected wavelengths (B) and corresponding DAS (C) obtained from global analysis. Transient absorption spectra of **1a**$^{\bullet+}$ in MeCN obtained *via* TA-SEC at selected delay times after excitation at 680 nm (D), kinetic traces at selected wavelengths (E) and corresponding DAS (F) obtained from global analysis.

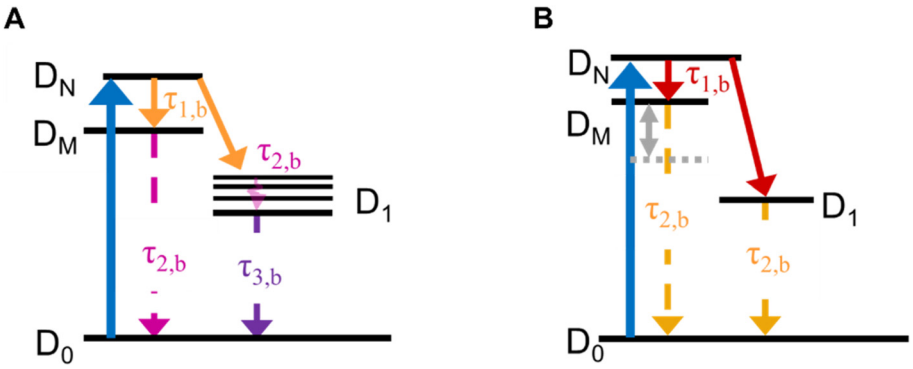

Fig. 8 Jablonski diagram showing the relaxation pathway of the radical cations (except for **1f**$^{\bullet+}$) upon excitation at 473 nm in acetonitrile (A). Jablonski diagram showing the relaxation pathway of **1f**$^{\bullet+}$ upon excitation at 473 nm in tetrahydrofuran (B).

value of $\tau_{1,b}$, we assign the corresponding molecular process to IC (see Fig. 8). The remaining characteristic time constant $\tau_{2,b}$ seems to originate from excited-state branching and to be related to an additional state D_M, which is only populated from higher-lying excited states. Further studies are required to characterise this additional state in detail.

The excited-state behaviours of **1d**$^{\bullet+}$ (see Fig. 9) and the alkyl-substituted **1e**$^{\bullet+}$ (see Fig. S28) resembles those of **1a**$^{\bullet+}$. In addition to the spectral features, *i.e.*, ESA maxima at 380 nm and 490 nm and GSB between 410 and 480 nm, the excited-state dynamics are also excitation wavelength-dependent. As before, this conclusion is based on the differing peak ratios found for excitation in the blue and in the red spectral region and on the fit of the data. Data obtained upon excitation at 680 nm are best fitted by a sum of two exponentials, while the data upon excitation at 470 nm are best fitted by a sum of

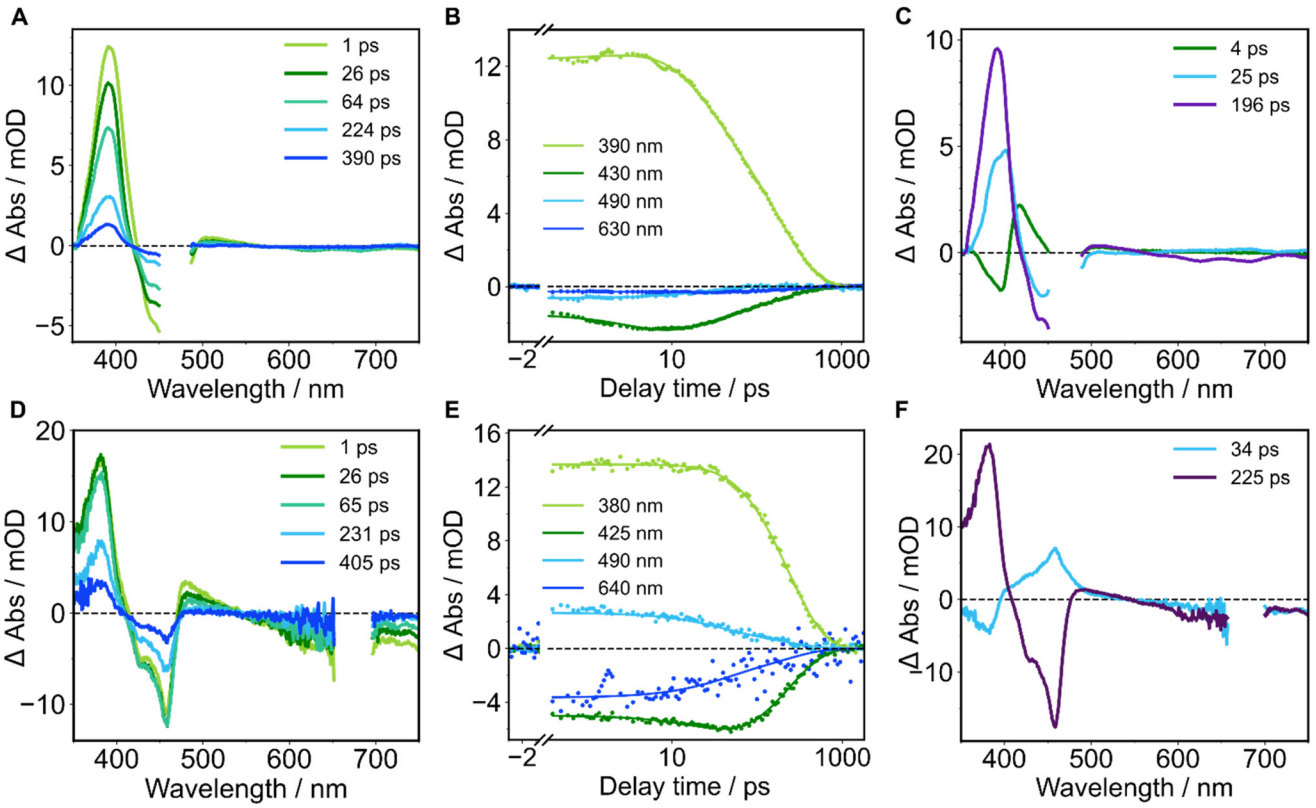

Fig. 9 Transient absorption spectra of **1d**$^{\bullet+}$ in MeCN obtained *via* TA-SEC at selected delay times after excitation at 460 nm (A), kinetic traces at selected wavelengths (B) and corresponding DAS (C) obtained from global analysis. Transient absorption spectra of **1d**$^{\bullet+}$ in MeCN obtained *via* TA-SEC at selected delay times after excitation at 680 nm (D), kinetic traces at selected wavelengths (E) and corresponding DAS (F) obtained from global analysis.

three exponentials. In both cases, the longest characteristic time constant has similar values and DAS. Therefore, ground-state recovery takes place from the same excited state, regardless of the excitation wavelength. Following the same argumentation as above, $\tau_{1,r}$ is assigned to relaxation within the D_1 state. Since the DAS of the two characteristic time constants $\tau_{1,b}$ and $\tau_{2,b}$ do not match the DAS obtained upon 680 nm excitation, it seems that relaxation also takes place *via* an additional, higher-lying state D_M in **1d**$^{\bullet+}$ and **1e**$^{\bullet+}$.

The same spectral features are observed for **1f**$^{\bullet+}$ as for the other radical cations (see Fig. S27). The data can be best fitted by a sum of two exponentials, irrespective of the excitation wavelengths. Furthermore, both the characteristic time constants $\tau_{2,b}$ = 89 ps and $\tau_{2,r}$ = 109 ps and the corresponding DAS obtained for **1f**$^{\bullet+}$ deviate from each other. For excitation at 470 nm, the DAS exhibits a broader negative feature that obscures the ESA maximum around 500 nm. These spectral differences suggest that $\tau_{2,b}$ rather describes a combination of both slow processes, *i.e.*, depopulation of the D_M state and ground-state recovery from the D_1 state, observed in the other radical cations (see Fig. 8B). Due to the poor solubility of **1f** in MeCN, the measurements of this compound were carried out in THF. Therefore, it is likely that observing only two processes upon blue excitation, as opposed to three processes for the other radical cations, is a consequence of the solvent change and not an inherent property of the compound itself. One possible explanation is that the D_M state is polar, and therefore less stable in the less polar THF, so depopulation of the state is slowed down according to the energy gap law. Consequently, depopulation of the D_M state proceeds with a similar time constant to depopulation of the D_1 state.

The fact that all of the radical cations investigated here exhibit spectral behaviour that is very similar to that of the alkyl-substituted derivative indicates that the change in charge distribution upon oxidation is mostly limited to the phenazine core. Therefore, it is the phenazine moiety that determines the spectral features in the region probed. Nevertheless, TA experiments revealed differences in the lifetimes of the radical species (see Table 3). Considering the results at hand, electron-donating substituents appear to extend the lifetime of the excited state, whereas electron-withdrawing substituents have the opposite effect. Furthermore, the decrease in excited-state lifetime is comparatively pronounced for **1a**$^{\bullet+}$. We assume that geometrical factors accelerate relaxation to the ground state even further. As previously discussed, a hydrogen bond between the pyridine nitrogen and a phenazine hydrogen might prevent significant structural changes, leading to faster relaxation.

Table 3 Excited-state lifetimes of the radical cations of compounds **1a**, **1b**, and **1d–f** obtained from TA-SEC measurements with an excitation wavelength of 680 nm

	1a$^{\bullet+}$	**1b**$^{\bullet+}$	**1d**$^{\bullet+}$	**1e**$^{\bullet+}$	**1f**$^{\bullet+}$
τ/ps	62	148	225	188	109

In general, excited states of radical cations exhibit very short lifetimes. For instance, triarylamine derivatives (pioneered by Koenig and co-workers) display excited-state lifetimes of approximately 10 ps.[35] Similarly, the photoexcited radical cation of PTH has a reported lifetime of up to 36 ps,[36,37] while structural modifications of PTH have extended this to as much as 1.8 ns.[37] To the best of our knowledge, excited-state lifetime studies for 5,10-dihydrophenazine radical cations remain limited. However, compared to other reported organic radical cations and anions,[38] the herein reported 5,10-dihydrophenazine radical cations exhibit notably longer excited-state lifetimes, ranging from 62 ps to 225 ps. This extended lifetime enhances their potential utility as effective photooxidants in photoredox catalysis.

Catalysis studies I: excited phenazine (1*) as electron donor

Reactive aryl radicals are key intermediates in numerous arylation reactions across various branches of chemistry, including organic synthesis, agricultural chemistry, and medicinal chemistry. One major advantage of using aryl radicals is the broad range of accessible precursors, such as aryl diazonium salts,[39] aryl halides,[40] and other aryl derivatives. Notable examples include the Sandmeyer reaction,[41] and the Meerwein arylation,[42] both of which utilize transition metal compounds (typically copper(I) complexes) to catalyze aryl radical formation from diazonium salts.[43] In contrast, the reduction of aryl halides is more chemically demanding due to their high thermodynamic stability and strongly negative reduction potentials.[44] Consequently, single-electron reduction of aryl halides is significantly more challenging than (for instance) that of aryl diazonium salts,[45] and often requires stoichiometric amounts of toxic reagents such as AIBN/*n*-Bu_3SnH.[40] These drawbacks have spurred the development of modern strategies, including photochemistry,[46] photoredox catalysis,[16,47–52] electrochemistry,[53] and hybrid electro-photochemical approaches.[54,55] Among these, organophotoredox catalysis has emerged as particularly promising, offering several advantages. This method operates under mild conditions and avoids the need for toxic or expensive transition or rare-metal catalysts. Furthermore, it requires only catalytic amounts of reagents compared to traditional stoichiometric reductive methods. Most importantly, upon light activation, many organic photoredox catalysts can achieve highly negative reduction potentials, often exceeding those of aryl bromides and chlorides, which are typically resistant to reduction by classical means.[40,44,53] Thus, photoreduction of aryl halides represents an effective approach to aryl radical generation.

As noted earlier, 5,10-dihydrophenazine cores have recently gained attention as potent organic photoreductants, particularly through the work of the Miyake group.[7,9] However, their potential for the reduction of aryl halides remains unexplored. To assess this capability, we investigated the performance of catalysts **1** in the reductive dehalogenation of aryl iodides. We first selected *p*-iodoanisole (**2a**) as the aryl radical precursor for the photoinduced deiodination reaction (Table 4). The model reaction employed **1a** as the photocatalyst, Cs_2CO_3 as the base,

Table 4 Conditions and catalyst screening for the reductive dehalogenation of *p*-iodoanisole **2a** mediated by **1**[a]

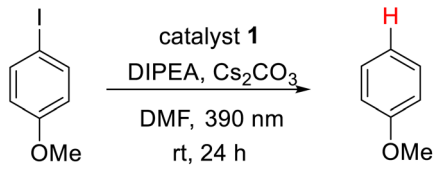

2a **3a**

Entry	Catalyst	Cs_2CO_3 (eq.)	DIPEA (eq.)	Yield **3a** (%)
1[b]	**1a**	1	3	32
2[b]	**1a**	0	3	33
3[b]	**1a**	1	0	22
4	**1a**	1	6	39
5	**1d**	1	6	39
6	**1f**	1	6	34
7	**1a**	0	6	53
8	**1d**	0	6	31
9	**1f**	0	6	22
10	**1a**	1	0	19
11	**1a**	0	0	11
12	None	1	6	24

[a] Reaction conditions (unless noted otherwise): **2a** (0.5 mmol, 1.0 eq.), catalyst (10 mol%), room temperature, DMF, 390 nm irradiation under argon atmosphere, 24 hours. Yields were determined from crude ^{1}H-NMR spectra using CH_2Br_2 as internal standard. [b] Under air, using 8 mol% of catalyst.

and *N*,*N*-diisopropylethylamine (DIPEA) as the sacrificial electron donor in DMF under 390 nm LED irradiation. We hypothesized that Cs_2CO_3 would serve primarily as a counterion source, releasing carbonate ions in DMF to stabilize the corresponding radical cation (**1a**$^{\bullet+}$). Initial experiments were conducted under ambient atmosphere (entries 1–3, Table 4).

Under these conditions, the desired product **3a** was obtained in 32% yield (entry 1). Interestingly, omitting the carbonate had little impact on the yield (33%, entry 2), suggesting no or only a limited role in promoting the reaction. However, removing DIPEA resulted in a lower yield of 22% (entry 3), though this outcome was not reproducible (see SI). These observations led us to suspect that even trace amounts of oxygen in the vial headspace may interfere with the photocatalytic cycle, potentially by oxidizing the excited state **1a***. To test this hypothesis, we switched to an inert argon atmosphere to exclude oxygen and ensure consistent catalytic performance, systematically varying catalyst and DIPEA loadings (entries 4–6, Table 4). Under these conditions, using 10 mol% of each catalyst (**1a**, **1d**, and **1f**) gave comparable yields of product **3a** (39%, 39%, and 34%, respectively). Notably, a significant increase in yield to 53% was observed when catalyst **1a** was used without Cs_2CO_3 and 6 instead of 3 equiv. DIPEA (entry 7, Table 4). However, this improvement was not mirrored with catalysts **1d** and **1f** under the same conditions: catalyst **1d** maintained a similar yield of 31% (entry 8), while **1f** gave a reduced yield of 22% (entry 9).

To investigate the role of DIPEA, we performed a control reaction in its absence, which resulted in a notable decrease in yield to 19% (entry 10). Similarly, when only catalyst **1a** and substrate **2a** were used (without any base or sacrificial donor), the yield dropped further to just 11% (entry 11). Interestingly, a reaction conducted without any catalyst still produced 24% of the product (entry 12), indicating the presence of a background reaction likely driven by direct photoactivation of the substrate. These findings suggest that both the photocatalyst and DIPEA can enhance the efficiency of the dehalogenation process, while Cs_2CO_3 plays a comparatively minor role. However, given the extent of the uncatalyzed background reactivity observed with **2a**, we turned our attention to a different substrate to more clearly assess the capacity of the catalysts to promote aryl radical generation (Table 5).

To evaluate the formation of aryl radicals, we employed an intramolecular radical cyclization strategy based on the principles established by Beckwith.[56] According to these rules, ring closures are classified as '*exo*' or '*endo*' depending on whether the newly formed bond lies outside or inside the ring, respect-

Table 5 Intramolecular radical cyclization experiments mediated by **1**[a]

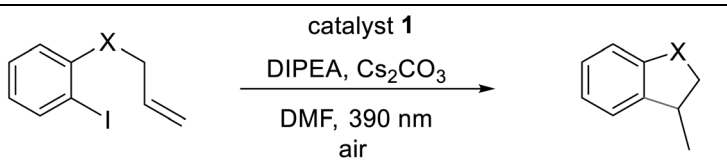

2b: X = O
2c: X = NBoc

3b: X = O
3c: X = NBoc

Entry	Substrate	Cs_2CO_3 (eq.)	Catalyst	Yield **3** (%)
1	**2b**	0	**1a**	0
2[b]	**2b**	1	**1a**	0
3[c]	**2c**	1	**1a**	65
4	**2c**	0	**1a**	56
5[c]	**2c**	1	**1f**	46

[a] Reaction conditions (unless noted otherwise): **2** (0.5 mmol, 1.0 eq.), catalyst (10 mol%), DIPEA (6 eq.), room temperature, DMF, 390 nm irradiation under air atmosphere, 20 hours. Isolated yields. [b] 10 eq. of DIPEA in 24 hours. [c] 17 hours.

ively. Generally, *exo-trig* cyclizations are kinetically favored over their *endo* counterparts.[56] Thus, we selected substrates specifically designed for radical cyclization, such as *ortho*-iodo derivatives of phenol or aniline bearing an allyl substituent. In these systems, the aryl radicals generated upon dehalogenation were expected to undergo preferential 5-*exo-trig* cyclization with the allyl group, yielding five-membered heterocycles. Allyl ether **2b**, which contains a phenolic ether group and resembles *p*-anisole **2a**, was chosen as the initial test substrate due to its structural similarity and its dual role as both radical precursor and radical trap. However, under standard conditions, the desired cyclized product **2b** was not observed (entry 1, Table 5). The addition of Cs_2CO_3 or increasing the DIPEA loading to 10 equivalents failed to improve the outcome (entry 2, Table 5). We hypothesized that the electron-donating nature of the phenol ether in **2b** might destabilize the aryl radical intermediate generated upon deiodination, thus impeding the expected cyclization. To overcome this, we turned to substrate **2c**, which features an allyl group along with a Boc-protected amine. We anticipated that this substrate would be more readily reduced *via* single-electron transfer and form a more stabilized radical intermediate compared to **2b**. As expected, under identical conditions, substrate **2c** delivered the cyclized product **3c** in a moderate isolated yield of 65% (entry 3, Table 5), supporting the hypothesis that photocatalyst **1a** could promote the single-electron reduction of **2c** and subsequent aryl radical generation. In line with Beckwith's rules, the aryl radical underwent an efficient 5-*exo-trig* cyclization with the allyl group to form the final product. Interestingly, omitting Cs_2CO_3 from the reaction led to a slightly reduced but still good yield of 56% (entry 4, Table 5). However, replacing catalyst **1a** with **1f** under the same conditions resulted in a lower yield of 46% (entry 5, Table 5), further highlighting the superior performance of catalyst **1a** in promoting aryl radical cyclization.

Considering the proposed mechanism for the deiodination of substrate **2a** (Fig. 10A), it is plausible that the excited state of catalyst **1a** ($E(\mathbf{1a}^*/\mathbf{1a}^{\bullet+})$ = −2.38 V *vs.* SCE) facilitates a single-electron transfer (SET) to substrate **2a** ($E(\mathbf{2a}/\mathbf{2a}^{\bullet-})$ = −2.03 V *vs.* $Ag/AgNO_3$ or −1.73 V *vs.* SCE).[49] In this process, the excited state **1a*** is quenched by **2a** *via* electron donation, forming the radical cation $\mathbf{1a}^{\bullet+}$ and the radical anion $\mathbf{2a}^{\bullet-}$. The latter undergoes C(sp^2)–I bond cleavage, generating an iodide ion (I^-) and an aryl radical ($\mathbf{2a}^{\bullet}$). To close the catalytic cycle, DIPEA acts as a sacrificial electron donor, reducing $\mathbf{1a}^{\bullet+}$ back to its neutral form (**1a**), while generating the radical cation $DIPEa^{\bullet+}$. The aryl radical $\mathbf{2a}^{\bullet}$ then undergoes hydrogen atom transfer (HAT) with $DIPEa^{\bullet+}$, leading to the formation of the final deiodinated product **3a** and the DIPEA iminium salt.[50,57] In contrast, when using substrate **2c**, the aryl radical generated under similar SET conditions follows a different pathway (Fig. 10B). Rather than undergoing hydrogen atom abstraction, the aryl radical engages in an intramolecular cyclization with the pendant allyl group, forming a cyclic radical intermediate. This intermediate can subsequently abstract a hydrogen atom from $DIPEa^{\bullet+}$, yielding the final *exo*-cyclic product **3c**.[49,50,57]

Catalysis studies II: excited phenazinium radical cation ($[\mathbf{1}^{\bullet+}]^*$) as electron acceptor

As discussed above, CV revealed that the one-electron oxidation processes of *N*,*N*-disubstituted-5,10-dihydrophenazines are chemically reversible, meaning that electro-generated cation radicals are stable on the timescale of the CV experiment. Additionally, SEC analysis confirmed that the resulting radical cations in their ground states absorb visible light. Based on these findings, we hypothesized that the excited radical cation of *N*,*N*-disubstituted-5,10-dihydrophenazines ($[\mathbf{1}^{\bullet+}]^*$) could serve as a strong photooxidant under visible light, enabling catalytic turnover through a reductive quenching pathway. To test this hypothesis, we selected the aerobic photooxidative C–H cyanation of *N*-aryl-1,2,3,4-tetrahydroisoquinolines (**4**) as a model reaction.[22] The 1,2,3,4-tetrahydroisoquinoline scaffold, a key structural motif in natural products and pharmaceutical agents with notable biological activity,[58] is also a common model substrate in oxidative transformations, as it features a nitrogen atom that can act as an electron donor in photoredox cycles.[22,59,60] In this case, we used molecular oxygen as an external oxidant to generate the radical cation *in situ* and irradiated the reaction mixture at 440 nm using an LED lamp.

Initial experiments were conducted using *N*-phenyl-1,2,3,4-tetrahydroisoquinoline (**4a**), trimethylsilyl cyanide (TMSCN), and catalyst **1a** under O_2 (Fig. 11). In the absence of catalyst, **5a** still formed with 34% yield, together with 11% of **6a**, indicating a considerable background reactivity. In the presence of **1a**, the desired cyanation product **5a** and the amide side-product **6a** were formed in 45% and 19% yields, respectively, with 92% of substrate **4a** consumed. Increasing the TMSCN loading to 2.0 equivalents led to reduced yields and lower conversion. However, further increasing TMSCN to 4.0 equivalents resulted in an improved yield of **5a** (77%) and complete substrate conversion, while suppressing the formation of **6a** to 3%. Notably, even with full conversion at 5.0 equivalents of TMSCN, no further improvement in **5a** yield was observed, and the yield of **6a** increased to 24%. A prolonged reaction (48 h) using 1.0 equivalent of TMSCN led to full conversion, yielding **5a** and **6a** in 63% and 5%, respectively (see SI for details). These results confirm that the model reaction can be effectively catalyzed by the dihydrophenazine core.

Encouraged by this outcome, we screened further catalysts to identify candidates with improved performance. Using the optimal TMSCN loading established with **1a**, a range of yields for **5a** was observed depending on the used catalyst (see SI for details). Catalysts **1d** and **1f** both enabled complete conversion of **4a** with high chemoselectivity, outperforming **1a**. This enhanced activity was attributed to the electron-donating groups or extended π-conjugation in **1d** and **1f**. Conversely, catalysts **1e** (lacking π-delocalized groups) and **1g** (monosubstituted with one electron-withdrawing group) gave lower yields and reduced conversion, likely due to unfavorable excited-state properties that limit catalytic efficiency. More specifically, the excited-state lifetime of $\mathbf{1a}^{\bullet+}$ was shown to be the shortest

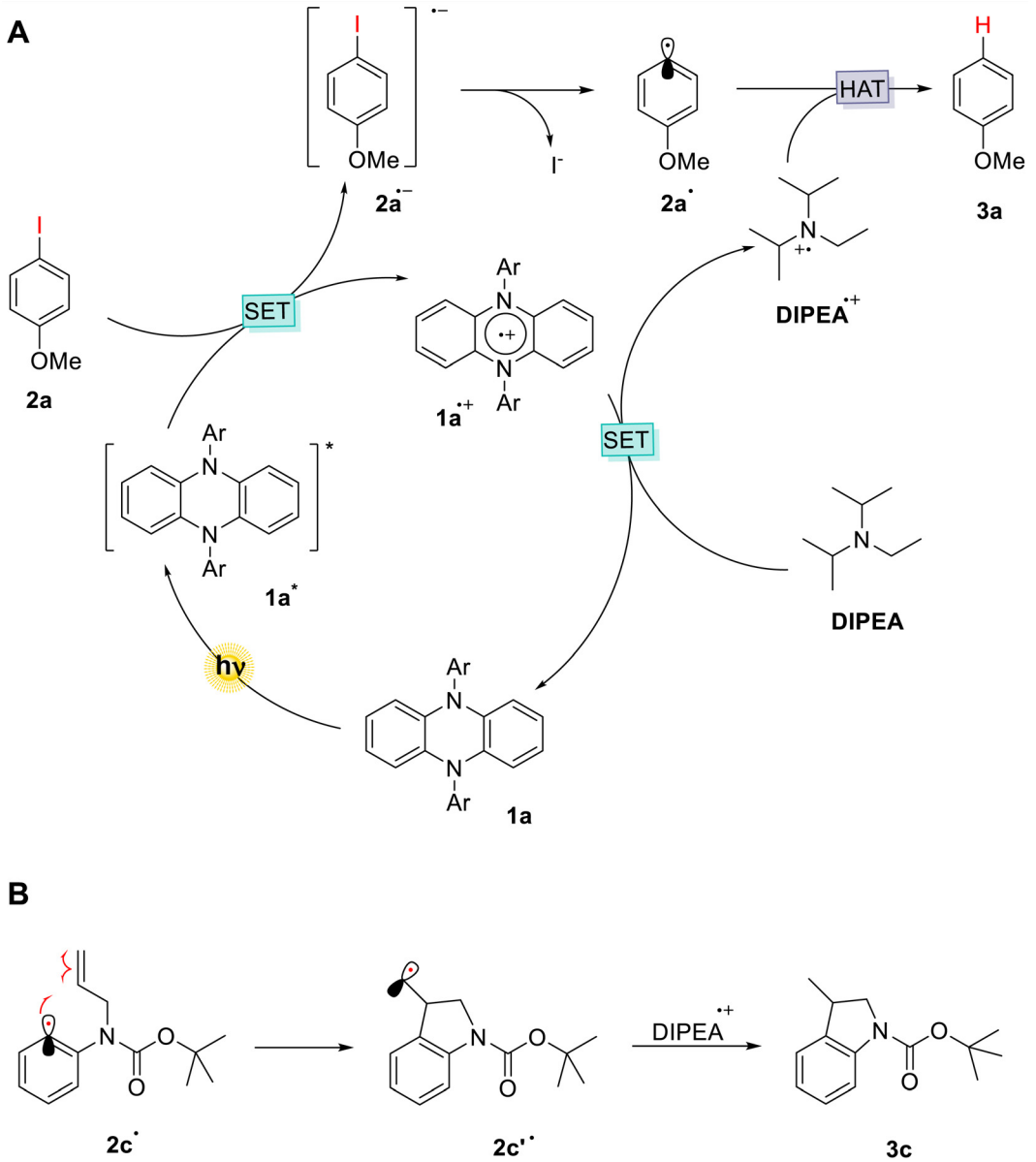

Fig. 10 Proposed reaction mechanism for the reductive deiodination of **2a** (A) and the radical cyclization of **2c** (B).

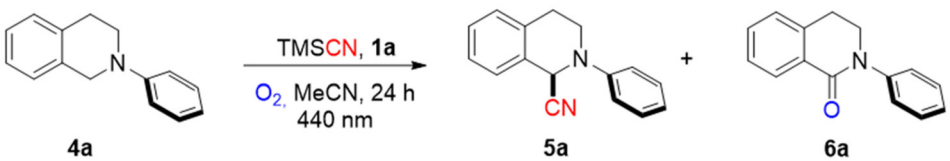

Fig. 11 Photooxidative aerobic C–H cyanation of *N*-phenyl-1,2,3,4-tetrahydroisoquinolines (**4a**) promoted by **1a**.

among the catalyst series. For **1e**, the correlation of the catalytic yield and the excited-state lifetime of the radical cation is not as straightforward. This suggests that additional factors, *e.g.* the excited-state geometry, redox potentials, and the exact reaction pathway play a role. This will be further discussed below. Given its superior performance, catalyst **1d** was selected for further optimization. Reducing the catalyst loading resulted in lower yields of **5a**, identifying 5 mol% as the optimal amount for this transformation. To assess the necessity of oxygen, we performed a control reaction under an anaerobic atmosphere. No product formation was observed, and the starting material remained intact. From these studies,

the optimal conditions for the model reaction were established. With these, we next investigated the substrate scope to assess the electronic and steric effects of various substituents on the benzene ring (Table 6).

The electronic nature of the substituents on the *N*-aryl ring of the substrates was found to have only a modest effect on the reaction outcome. Substrates bearing electron-rich aryl groups, such as a *p*-methoxyphenyl, delivered the desired product **5c** in good yield (82%). In comparison, slightly diminished yields were observed with electron-deficient aryl groups. For example, substrates featuring *p*-trifluoromethyl and carboxyl substituents afforded products **5e** and **5f** in 76% and 58% yields, respectively. These results suggest that while the reaction tolerates a broad range of electronic environments, electron-rich systems slightly promote the transformation, likely due to enhanced stabilization of radical intermediates and/or improved oxidizability.

In addition to electronic effects, our investigation revealed that the position of substituents on the aryl ring significantly impacts reaction efficiency, pointing to a steric component. To assess this, we examined substrates bearing methyl groups at different positions on the benzene ring. The *para*-substituted

Table 6 Photooxidative C–H cyanation of *N*-aryl-1,2,3,4-tetrahydroisoquinolines (**4**) mediated by **1d** [a,b,c]

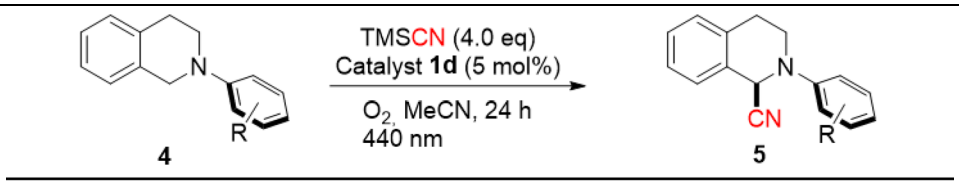

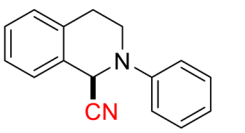
5a, 90%

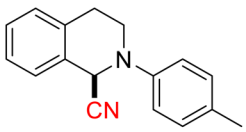
5b, 77%

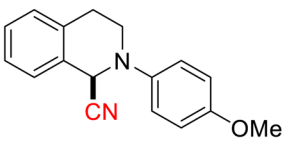
5c, 82%

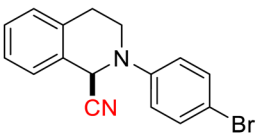
5d, 73%

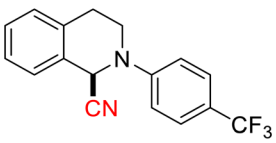
5e, 76%

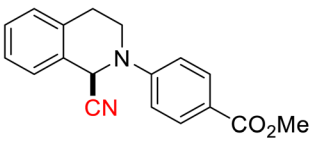
5f, 58%[b]

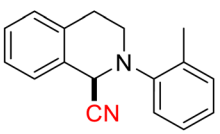
5g, 55%

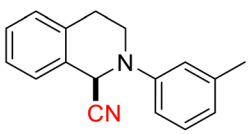
5h, 67%

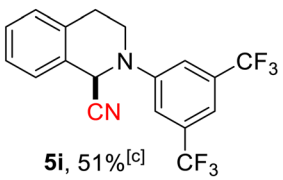
5i, 51%[c]

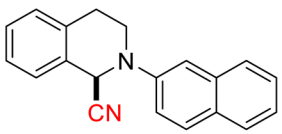
5j, 83%

[a] Reaction conditions: 5 mol% of catalyst **1d**, 4.0 equivalents of TMSCN, and 1.0 equivalent of substrate **4** in 2 mL MeCN under an O_2 atmosphere with 440 nm irradiation. Average isolated yield from triplicate reactions. Complete experimental details for each product can be found in the SI. [b] Yield from a single reaction. [c] Average isolated yield from two reactions.

substrate delivered product **5b** in 77% yield, while the *meta*- and *ortho*-substituted analogues **5h** and **5g** gave lower yields of 67% and 55%, respectively. These results suggest that steric hindrance, particularly from *ortho*-substituents, impedes the nucleophilic attack on reactive intermediates or reduces access to productive geometries for catalyst–substrate interactions.

To gain deeper mechanistic insight of this transformation, radical scavengers such as 2,2,6,6-tetramethylpiperidine-1-oxyl (TEMPO) and 2,6-di-*tert*-butyl-4-methylphenol (BHT) were introduced into the model reaction. In both cases, the formation of the desired product was completely suppressed, suggesting the involvement of a radical pathway. To further probe this mechanism and detect radical species, we conducted electron paramagnetic resonance (EPR) studies under standard reaction conditions (*vide infra*).

The ground-state oxidation potential of catalyst **1d** (E(**1d**/**1d**$^{\bullet+}$) = +0.16 V *vs.* SCE) is insufficient to reduce molecular oxygen (O_2), which has a reduction potential of $E(O_{2(g)}/O_2^{\bullet-})$ = −0.88 V *vs.* SCE (in MeCN).[61] This unfavorable thermodynamic profile suggests that the reaction likely proceeds *via* the photoexcited state of the catalyst. Upon photoexcitation, molecules typically exhibit altered electronic configurations, which can drastically modify their redox properties. Based on this, we hypothesized that catalyst **1d** is promoted to its excited state (**1d***) under irradiation, enabling a single-electron transfer (SET) to molecular oxygen. This step would generate the superoxide radical anion ($O_2^{\bullet-}$) and the radical cation **1d**$^{\bullet+}$. To evaluate the feasibility of this step, we estimated the excited-state redox potential of **1d** using the Stokes shift (see SI for details).[11] This value allowed us to approximate the excited-state redox potential of the pair **1d***/**1d**$^{\bullet+}$ as −2.81 V *vs.* SCE, indicating that SET to oxygen is thermodynamically favorable.

On the one hand, catalyst turnover is not prone to occur through reduction of the radical cation **1d**$^{\bullet+}$ by the substrate **4a**, returning the catalyst to its neutral state. This step is thermodynamically unviable, as shown by the redox potentials of **1d**/**1d**$^{\bullet+}$ (+0.16 V *vs.* SCE) and **4a**/**4a**$^{\bullet+}$ (+1.04 V *vs.* SCE) in MeCN.[62] On the other hand, based on photophysical analysis, it is possible that the excited radical cation ([**1d**$^{\bullet+}$]*) participates in this turnover step. The redox potential of the [**1d**$^{\bullet+}$]*/**1d** couple was estimated at +1.84 V *vs.* SCE (see SI), which supports the feasibility of SET from **4a** to the excited-state radical cation [**1d**$^{\bullet+}$]*, resulting in the formation of the tertiary amine radical cation **4a**$^{\bullet+}$. According to prior studies,[22,59,60,63] this radical cation undergoes hydrogen atom abstraction at the benzylic position by the superoxide radical anion ($O_2^{\bullet-}$),

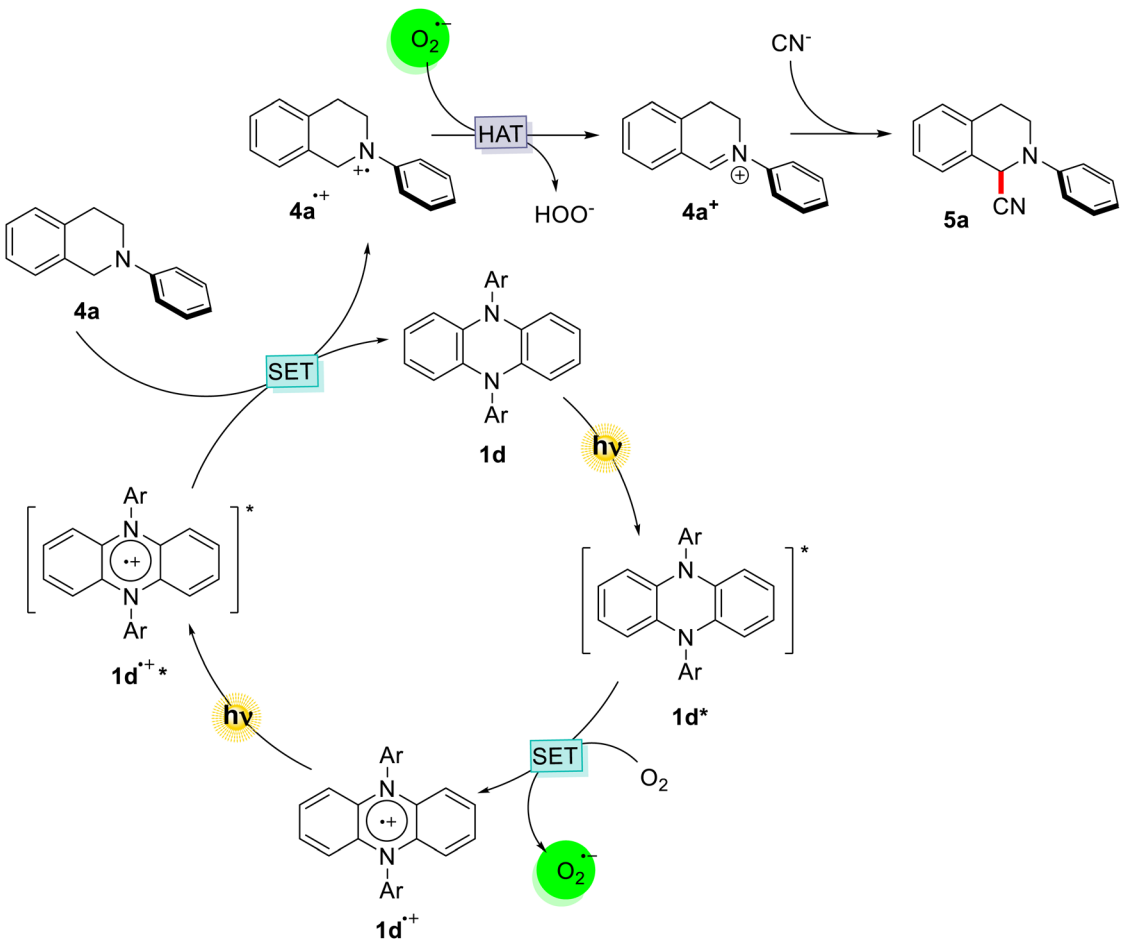

Fig. 12 Proposed reaction mechanism *via* single electron transfer (SET) for the photooxidative aerobic C–H cyanation of **4a** promoted by **1d**.

forming a hydroperoxide anion (HOO^-) and the corresponding iminium intermediate **4a**$^+$. This intermediate is then trapped by cyanide (CN^-) from TMSCN, yielding the final product **5a** (Fig. 12).

Alternatively, the reaction may proceed through an energy transfer (ET) pathway involving sensitization of molecular oxygen. In this mechanism, energy transfer from the excited triplet state of catalyst **1d** to ground-state triplet oxygen ($^3O_2$) produces singlet oxygen ($^1O_2$).[59] Notably, the one-electron oxidation of electron-rich compounds by $^1O_2$ is generally more favorable than by $^3O_2$.[64] Consequently, substrate **4a** may undergo oxidation by $^1O_2$ *via* a proton-coupled electron transfer (PCET) process, yielding the aryl radical intermediate **4a**$^\bullet$ and a hydroperoxyl radical ($HOO^\bullet$). These radical species can then engage in a cross-coupling reaction to form intermediate product 7, which, upon protonation, releases hydrogen peroxide (H_2O_2), generating the iminium-like intermediate **4a**$^+$. Alternatively, **4a**$^+$ may also form through a second step in which $HOO^\bullet$ abstracts an electron from the radical intermediate **4a**$^\bullet$. Regardless of the specific pathway, intermediate **4a**$^+$ subsequently reacts with cyanide (CN^-) to afford the final product **5a** (Fig. 13).

Additional EPR experiments were conducted to gain deeper insight into the reaction mechanism. In the presence of O_2, the EPR spectrum of the reaction mixture prior to irradiation displayed a signal corresponding to the phenazine radical cation of photocatalyst **1d**, characterized by g = 2.004 and a hyperfine splitting of 2 × A_N = 6.53 G (Fig. 14, black trace; simulated spectrum in Fig. S21a).[20] As previously discussed, the spontaneous single-electron transfer (SET) from catalyst **1d** to molecular oxygen generating the radical cation **1d**$^{\bullet+}$ is thermodynamically unfavorable. However, this process can still proceed when the generated superoxide anion ($O_2^{\bullet-}$) is removed from the equilibrium by an irreversible follow-up reaction. The high reactivity of $O_2^{\bullet-}$ allows it to quickly react with protic substances (such as adventitious moisture or other proton donors present in the reaction mixture),[65] a phenomenon well documented in earlier studies.[20,22] Consequently, the detection of **1d**$^{\bullet+}$, particularly in the early stages of the reaction, supports the feasibility of the SET pathway, as illustrated in Fig. 12. Notably, the intensity of the EPR signal of **1d**$^{\bullet+}$, gradually diminished and nearly disappeared within the first hour of irradiation in the absence of oxygen (Fig. S19b), supporting the key role of oxygen in the reaction mechanism.

Upon short-term irradiation, the use of DMPO as a spin-trapping reagent revealed the formation of the DMPO–$^\bullet$OOH spin adduct, followed by the detection of a carbon-centered radical DMPO adduct (Fig. S20 and S22). The appearance of the [DMPO–OOH]$^\bullet$ adduct indicates the presence of superoxide radicals generated during the photoreaction.[66] Furthermore, after irradiation, the EPR spectrum of the reaction mixture displayed a characteristic 14-line signal (g = 2.004; A_N = 15.75 G, 2 × A_H = 11.11 G, 2 × A_H = 6.24 G, A_H = 5.36 G), consistent with the formation of the aryl radical intermediate **4a**$^\bullet$ (Fig. 14, red

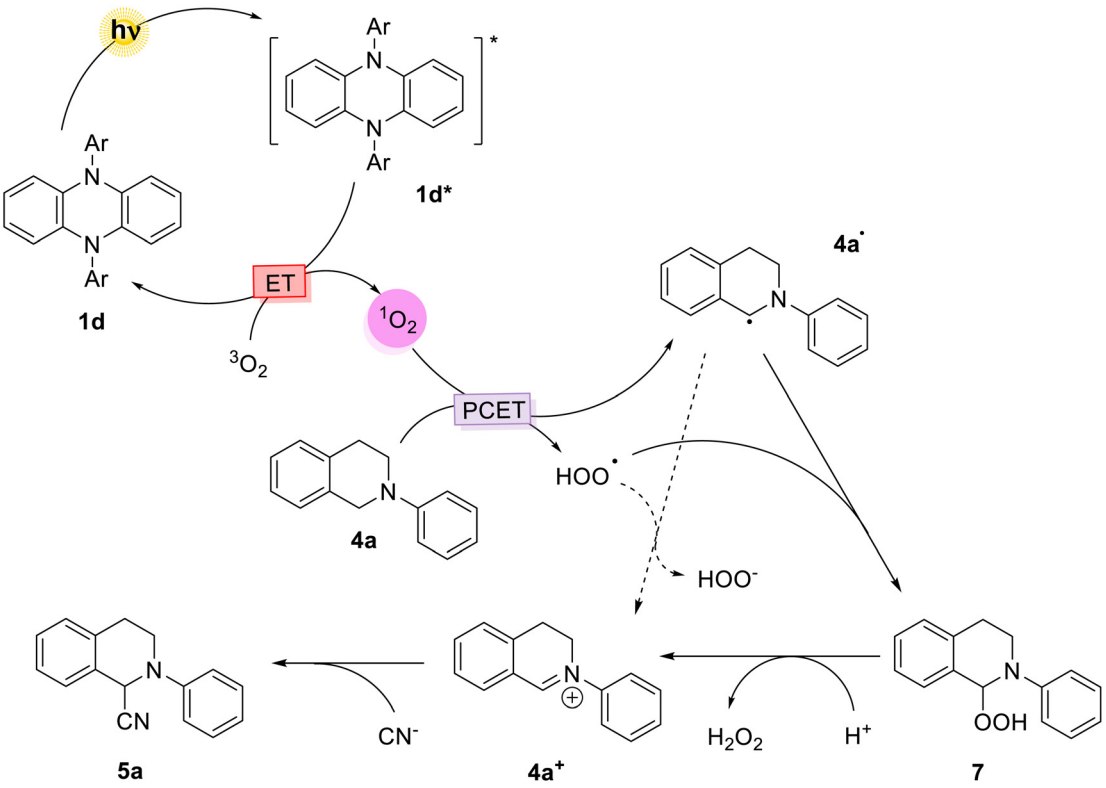

Fig. 13 Proposed alternative reaction mechanism *via* sensitization of molecular oxygen through energy transfer (ET) for the photooxidative aerobic C–H cyanation of **4a** promoted by **1d**.

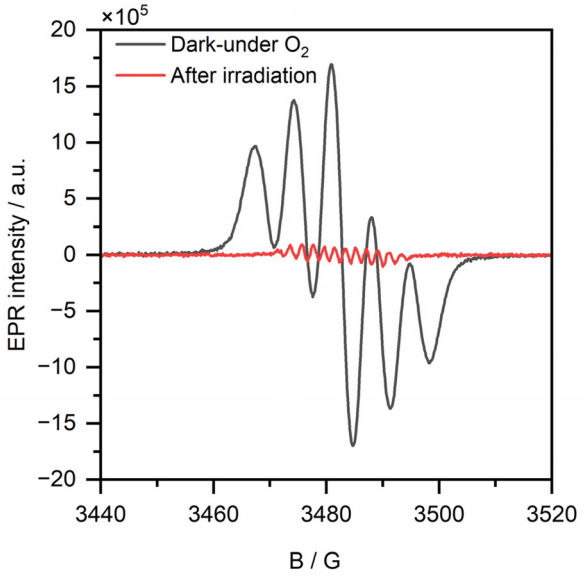

Fig. 14 EPR spectra of reaction mixture for photooxidative cyanation of **4a** promoted by **1d** under O_2 flow in the dark (black trace) and after 1 hour of irradiation (red trace) at room temperature.

trace; simulated spectrum in Fig. S21b). It should be noted that the formation of **4a**$^{\bullet}$ is only observed in the presence of O_2 (Fig. S19a), well in agreement with the ET mechanism in Fig. 13.

To evaluate the feasibility of $^1O_2$-mediated oxidation, we replaced our catalyst with 5,10,15,20-tetraphenylporphyrin (TPP), a well-known photosensitizer with a long-lived triplet state and high quantum yield for $^1O_2$ generation.[67] Under these conditions, complete conversion of substrate **4a** was observed, and product **5a** was obtained in excellent yield (83%) (see SI), supporting the potential involvement of an ET pathway. However, literature reports that when the same $^1O_2$ generation system (TPP in dichloromethane) was applied to the more electron-rich substrate **4c**, no formation of product **5c** was observed despite full substrate consumption.[68] This suggests that although oxygen sensitization *via* ET (Fig. 13) can occur under the reaction conditions, it does not universally lead to productive outcomes. These findings support potential coexistence of both mechanistic pathways, the energy transfer (ET, Fig. 13) and the single-electron transfer (SET, Fig. 12), with the dominant mechanism likely dependent on the electronic nature of the substrate.

Conclusion

We developed a new class of organophotoredox catalysts based on the 5,10-dihydrophenazine core, functionalized with heterocycles serving as electron-withdrawing groups. These catalysts were comprehensively characterized using cyclic voltammetry (CV) and spectroelectrochemistry (SEC), providing insight into their redox behavior and photophysical properties. Excited-state analyses revealed that the catalysts act as potent photoreductants, enabling the activation of C(sp^2)–I bonds through single-electron transfer, thereby facilitating the generation of aryl radicals under visible-light irradiation. Beyond their reductive capabilities, the excited-state radical cations of these catalysts were shown to participate in oxidative transformations. This dual reactivity was exemplified in the oxidative C(sp^3)–H cyanation of tertiary amines, highlighting the Janus-type redox behavior of the system. Mechanistic studies, including electron paramagnetic resonance (EPR) spectroscopy and time-resolved transient absorption measurements, further confirmed the intermediacy of both radical species and the catalyst's role in the photoredox cycle.

Tentative structure–activity relationships of the dihydrophenazine derivatives can be correlated from their redox potentials, excited-state lifetimes and catalytic efficiencies (Tables 2 and 3). Catalysts **1d** and **1f** demonstrated exceptional performance in photooxidative cyanation, achieving yields of >99% and 99%, respectively. This high reactivity is likely due to their relatively high excited-state oxidation potentials ($E([\mathbf{1}^{\bullet+}]^*/\mathbf{1})$ = +1.84 V for **1d** and +1.65 V for **1f** *vs.* SCE) and long excited-state lifetimes (225 and 109 ps, respectively), promoting efficient single-electron oxidation of the amine substrate. In contrast, catalyst **1e** exhibited a lower oxidative yield of 48%, despite possessing the most reducing excited singlet state ($E(\mathbf{1}^*/\mathbf{1}^{\bullet+})$ = −2.93 V *vs.* SCE) and a long-lived excited radical cation (188 ps). This suggests that factors beyond redox potential, such as solubility or aggregation, may influence reactivity. In the photoreductive dehalogenation of aryl iodides, catalyst **1a** produced a yield of 53%, whereas **1e** and **1f** produced reduced yields of 31% and 22%, respectively. Interestingly, despite having the shortest excited-state lifetime (62 ps), 1a outperformed the other catalysts in the reductive process. This may reflect a favourable balance between its redox potential ($E(\mathbf{1}^*/\mathbf{1}^{\bullet+})$ = −2.38 V) and structural stability under reducing conditions. In contrast, the lower yields observed for **1e** and **1f** in deiodination reactions may be due to limited stability under photoreductive conditions rather than poor reactivity. Although our focus was on electronic and photophysical parameters, post-reaction analysis would be necessary to eliminate the possibility of these catalysts degrading during the reaction. This highlights the need for future studies to investigate catalyst stability and decomposition pathways under diverse photoredox conditions.

The unique redox flexibility of these phenazine-based catalysts positions them as promising candidates for a broader range of applications in challenging photoredox processes, beyond the specific transformations explored here. Their performance is comparable to that of state-of-the-art organic photocatalysts, such as phenothiazines, acridinium salts and carbazoles. They offer complementary excited-state potentials and longer-lived radical cation states. Their ability to engage in both oxidative and reductive quenching pathways under visible light distinguishes these catalysts, and future studies will seek to delineate their functional scope, limitations, and compatibility in more complex reaction systems. Collectively, these

findings establish 5,10-dihydrophenazine derivatives as versatile and tunable platforms for both reductive and oxidative photoredox catalysis, broadening the scope of metal-free photocatalytic transformations.

Author contributions

P. P. H. Q. conceived and designed the research, carried out the synthetic work, catalysis experiments, and data analysis. N. H. performed the spectroscopic investigations and data analysis. T. H. V. conducted the EPR experiments and contributed to data analysis. A. P. performed the electrochemical studies and data analysis. R. F. designed and supervised the electrochemical investigations and contributed to data analysis. B. D.-I. designed and supervised the spectroscopic investigations and contributed to data analysis. E. M. conceived and supervised the overall project and acquired funding. All authors contributed to writing and editing the manuscript.

Conflicts of interest

There are no conflicts to declare.

Data availability

The data supporting this article have been included as part of the supplementary information (SI). Supplementary information: general experimental details, synthesis and full characterization of 5,10-dihydrophenazine-based photocatalysts and catalysis substrates, single-crystal X-ray data, and procedures for photocatalytic dehalogenation and oxidative C(sp^3)–H cyanation. Extensive mechanistic studies (CV, SEC, EPR, and control experiments) are provided alongside complete spectral data (NMR, GC-MS). See DOI: **https://doi.org/10.1039/d5qo01348h**.

The authors have cited additional references within the SI.[11,20,24,43,66,69–91]

CCDC 2379436 and 2432793 contain the supplementary crystallographic data for this paper.[92a,b]

Acknowledgements

P. P. H. Q acknowledges the support from the RoHan Project funded by the German Academic Exchange Service (DAAD, No. 57315854 and 57560571) and the Federal Ministry for Economic Cooperation and Development (BMZ) inside the framework "SDG Bilateral Graduate School Programme". R. F. is grateful for financial support by the German Research Foundation (DFG Heisenberg Program, FR 3848/4-2). We also thank Dr Martina Beese (Institute of Mathematics, University of Rostock), Dr Anke Spannenberg, Dr Wolfgang Baumann and the Analytics Department at LIKAT for their helpful suggestions and technical support.

Artificial intelligence tools were employed during the preparation of this work. An illustrative image of the Roman god Janus, used in the graphical abstract, was generated using OpenAI's DALL·E. The image was created specifically for this work and is not based on any copyrighted source material. OpenAI's ChatGPT was also used to assist in grammar and language refinement of the manuscript. No sensitive, personal, or unpublished research data were input into the AI tool. The authors ensured that all data shared with ChatGPT complied with institutional and publisher privacy standards. All scientific content, data analysis, and final editorial decisions were made independently by the authors.

References

1 C. M. Friend and B. Xu, Heterogeneous Catalysis: A Central Science for a Sustainable Future, *Acc. Chem. Res.*, 2017, **50**, 517–521.
2 M. H. Shaw, J. Twilton and D. W. C. MacMillan, Photoredox Catalysis in Organic Chemistry, *J. Org. Chem.*, 2016, **81**, 6898–6926.
3 I. K. Sideri, E. Voutyritsa and C. G. Kokotos, Photoorganocatalysis, small organic molecules and light in the service of organic synthesis: the awakening of a sleeping giant, *Org. Biomol. Chem.*, 2018, **16**, 4596–4614.
4 T. Noël and E. Zysman-Colman, The promise and pitfalls of photocatalysis for organic synthesis, *Chem. Catal.*, 2022, **2**, 468–476.
5 S. G. E. Amos, M. Garreau, L. Buzzetti and J. Waser, Photocatalysis with organic dyes: facile access to reactive intermediates for synthesis, *Beilstein J. Org. Chem.*, 2020, **16**, 1163–1187.
6 S. P. Pitre, C. D. McTiernan and J. C. Scaiano, Library of Cationic Organic Dyes for Visible-Light-Driven Photoredox Transformations, *ACS Omega*, 2016, **1**, 66–76.
7 Y. Du, R. M. Pearson, C. H. Lim, S. M. Sartor, M. D. Ryan, H. Yang, N. H. Damrauer and G. M. Miyake, Strongly Reducing, Visible-Light Organic Photoredox Catalysts as Sustainable Alternatives to Precious Metals, *Chem. – Eur. J.*, 2017, **23**, 10962–10968.
8 D. A. Corbin, B. G. McCarthy, Z. van de Lindt and G. M. Miyake, Radical Cations of Phenoxazine and Dihydrophenazine Photoredox Catalysts and Their Role as Deactivators in Organocatalyzed Atom Transfer Radical Polymerization, *Macromolecules*, 2021, **54**, 4726–4738.
9 J. C. Theriot, C. H. Lim, H. Yang, M. D. Ryan, C. B. Musgrave and G. M. Miyake, Organocatalyzed atom transfer radical polymerization driven by visible light, *Science*, 2016, **352**, 1082–1086.
10 C. H. Lim, M. D. Ryan, B. G. McCarthy, J. C. Theriot, S. M. Sartor, N. H. Damrauer, C. B. Musgrave and G. M. Miyake, Intramolecular Charge Transfer and Ion Pairing in N,N-Diaryl Dihydrophenazine Photoredox

Catalysts for Efficient Organocatalyzed Atom Transfer Radical Polymerization, *J. Am. Chem. Soc.*, 2017, **139**, 348–355.

11 N. A. Romero and D. A. Nicewicz, Organic Photoredox Catalysis, *Chem. Rev.*, 2016, **116**, 10075–10166.

12 T. Bortolato, S. Cuadros, G. Simionato and L. Dell'Amico, The advent and development of organophotoredox catalysis, *Chem. Commun.*, 2022, **58**, 1263–1283.

13 Y. Lee and M. S. Kwon, Emerging Organic Photoredox Catalysts for Organic Transformations, *Eur. J. Org. Chem.*, 2020, 6028–6043, DOI: 10.1002/ejoc.202000720.

14 S. M. Sartor, B. G. McCarthy, R. M. Pearson, G. M. Miyake and N. H. Damrauer, Exploiting Charge-Transfer States for Maximizing Intersystem Crossing Yields in Organic Photoredox Catalysts, *J. Am. Chem. Soc.*, 2018, **140**, 4778–4781.

15 M. J. Price, K. O. Puffer, M. Kudisch, D. Knies and G. M. Miyake, Structure-property relationships of core-substituted diaryl dihydrophenazine organic photoredox catalysts and their application in O-ATRP, *Polym. Chem.*, 2021, **12**, 6110–6122.

16 I. Ghosh and B. König, Chromoselective Photocatalysis: Controlled Bond Activation through Light-Color Regulation of Redox Potentials, *Angew. Chem., Int. Ed.*, 2016, **55**, 7676–7679.

17 S. Doose, H. Neuweiler and M. Sauer, Fluorescence quenching by photoinduced electron transfer: a reporter for conformational dynamics of macromolecules, *ChemPhysChem*, 2009, **10**, 1389–1398.

18 K. Targos, O. P. Williams and Z. K. Wickens, Unveiling Potent Photooxidation Behavior of Catalytic Photoreductants, *J. Am. Chem. Soc.*, 2021, **143**, 4125–4132.

19 K. Ohkubo, T. Kobayashi and S. Fukuzumi, Direct oxygenation of benzene to phenol using quinolinium ions as homogeneous photocatalysts, *Angew. Chem., Int. Ed.*, 2011, **50**, 8652–8655.

20 R. Brisar, F. Unglaube, D. Hollmann, H. Jiao and E. Mejía, Aerobic Oxidative Homo- and Cross-Coupling of Amines Catalyzed by Phenazine Radical Cations, *J. Org. Chem.*, 2018, **83**, 13481–13490.

21 J. Y. Lin, Z. Y. Guo and H. B. Zhan, A robust phenazine-containing organic polymer as catalyst for amine oxidative coupling reactions, *J. Catal.*, 2020, **385**, 338–344.

22 F. Unglaube, P. Hünemörder, X. Guo, Z. Chen, D. Wang and E. Mejía, Phenazine Radical Cations as Efficient Homogeneous and Heterogeneous Catalysts for the Cross-Dehydrogenative Aza-Henry Reaction, *Helv. Chim. Acta*, 2020, **103**, e2000184.

23 B. Huang, H. Kang, X.-L. Zhao, H.-B. Yang and X. Shi, Redox Properties of N,N′-Disubstituted Dihydrophenazine and Dihydrodibenzo[a,c]phenazine: The First Isolation of Their Crystalline Radical Cations and Dications, *Cryst. Growth Des.*, 2022, **22**, 3587–3593.

24 M. Sawall, C. Ruckebusch, M. Beese, R. Francke, A. Prudlik and K. Neymeyr, An active constraint approach to identify essential spectral information in noisy data, *Anal. Chim. Acta*, 2022, **1233**, 340448.

25 R. E. Hester and K. P. J. Williams, Free-Radical Studies by Resonance Raman-Spectroscopy - the 5,10-Dihydrophenazine and 5-Methyl-10-Hydrophenazine Radical Cations, *J. Raman Spectrosc.*, 1982, **13**, 91–95.

26 L. Li, Y. Su, Y. Ji and P. Wang, A Long-Lived Water-Soluble Phenazine Radical Cation, *J. Am. Chem. Soc.*, 2023, **145**, 5778–5785.

27 J. D. Bell and J. A. Murphy, Recent advances in visible light-activated radical coupling reactions triggered by (i) ruthenium,(ii) iridium and (iii) organic photoredox agents, *Chem. Soc. Rev.*, 2021, **50**, 9540–9685.

28 A. Bhattacherjee, M. Sneha, L. Lewis-Borrell, G. Amoruso, T. A. A. Oliver, J. Tyler, I. P. Clark and A. J. Orr-Ewing, Singlet and Triplet Contributions to the Excited-State Activities of Dihydrophenazine, Phenoxazine, and Phenothiazine Organocatalysts Used in Atom Transfer Radical Polymerization, *J. Am. Chem. Soc.*, 2021, **143**, 3613–3627.

29 D. Koyama, H. J. A. Dale and A. J. Orr-Ewing, Ultrafast Observation of a Photoredox Reaction Mechanism: Photoinitiation in Organocatalyzed Atom-Transfer Radical Polymerization, *J. Am. Chem. Soc.*, 2018, **140**, 1285–1293.

30 Z. Zhang, Y. S. Wu, K. C. Tang, C. L. Chen, J. W. Ho, J. Su, H. Tian and P. T. Chou, Excited-State Conformational/Electronic Responses of Saddle-Shaped N,N'-Disubstituted-Dihydrodibenzo[a,c]phenazines: Wide-Tuning Emission from Red to Deep Blue and White Light Combination, *J. Am. Chem. Soc.*, 2015, **137**, 8509–8520.

31 Y. Hirata and I. Tanaka, Intersystem crossing to the lowest triplet state of phenazine following singlet excitation with a picosecond pulse, *Chem. Phys. Lett.*, 1976, **43**, 568–570.

32 R. B. Weerasooriya, M. C. Drummer, B. T. Phelan, J. L. Gesiorski, E. A. Sprague-Klein, L. X. Chen and K. D. Glusac, Toward Metal-free Photocatalysis: Photochemical Regeneration of Organic Hydride Donors Using Phenazine-Based Photosensitizers, *J. Phys. Chem. C*, 2022, **126**, 17816–17825.

33 B. McCarthy, S. Sartor, J. Cole, N. Damrauer and G. M. Miyake, Solvent Effects and Side Reactions in Organocatalyzed Atom Transfer Radical Polymerization for Enabling the Controlled Polymerization of Acrylates Catalyzed by Diaryl Dihydrophenazines, *Macromolecules*, 2020, **53**, 9208–9219.

34 R. K. Venkatraman and A. J. Orr-Ewing, Solvent Effects on Ultrafast Photochemical Pathways, *Acc. Chem. Res.*, 2021, **54**, 4383–4394.

35 B. Bieszczad, T. Karl, A. Rolka, P. Nuernberger, R. Kutta and B. Koenig, Oxidative con-PET Catalysis for Arene Functionalization, *ChemRxiv*, 2022, preprint, ChemRxiv:2022-39x5l, DOI:DOI: 10.26434/chemrxiv-2022-39x5l.

36 J. A. Christensen, B. T. Phelan, S. Chaudhuri, A. Acharya, V. S. Batista and M. R. Wasielewski, Phenothiazine Radical Cation Excited States as Super-oxidants for Energy-Demanding Reactions, *J. Am. Chem. Soc.*, 2018, **140**, 5290–5299.

37 F. Weick, N. Hagmeyer, M. Giraud, B. Dietzek-Ivansic and H. A. Wagenknecht, Reductive Activation of Aryl Chlorides

by Tuning the Radical Cation Properties of N-Phenylphenothiazines as Organophotoredox Catalysts, *Chem. – Eur. J.*, 2023, **29**, e202302347.

38 L. D. Mena, J. L. Borioni, S. Caby, P. Enders, M. A. Argüello Cordero, F. Fennel, R. Francke, S. Lochbrunner and J. I. Bardagi, Quantitative prediction of excited-state decay rates for radical anion photocatalysts, *Chem. Commun.*, 2023, **59**, 9726–9729.

39 C. Galli, Radical Reactions of Arenediazonium Ions - an Easy Entry into the Chemistry of the Aryl Radical, *Chem. Rev.*, 1988, **88**, 765–792.

40 H. G. Kuivila, Organotin hydrides and organic free radicals, *Acc. Chem. Res.*, 1968, **1**, 299–305.

41 T. Sandmeyer, Ueber die Ersetzung der Amidgruppe durch Chlor in den aromatischen Substanzen, *Ber. Dtsch. Chem. Ges.*, 1884, **17**, 1633–1635.

42 H. Meerwein, E. Büchner and K. van Emster, Über die Einwirkung aromatischer Diazoverbindungen auf α,β–ungesättigte Carbonylverbindungen, *J. Prakt. Chem.*, 1939, **152**, 237–266.

43 R. Akhtar, A. F. Zahoor, N. Rasool, M. Ahmad and K. G. Ali, Recent trends in the chemistry of Sandmeyer reaction: a review, *Mol. Divers.*, 2022, **26**, 1837–1873.

44 X. Tian, Y. Liu, S. Yakubov, J. Schutte, S. Chiba and J. P. Barham, Photo- and electro-chemical strategies for the activations of strong chemical bonds, *Chem. Soc. Rev.*, 2024, **53**, 263–316.

45 N. Kvasovs and V. Gevorgyan, Contemporary methods for generation of aryl radicals, *Chem. Soc. Rev.*, 2021, **50**, 2244–2259.

46 T. Kawamoto, A. Sato and I. Ryu, Photoinduced Aminocarbonylation of Aryl Iodides, *Chem. – Eur. J.*, 2015, **21**, 14764–14767.

47 J. D. Nguyen, E. M. D'Amato, J. M. Narayanam and C. R. Stephenson, Engaging unactivated alkyl, alkenyl and aryl iodides in visible-light-mediated free radical reactions, *Nat. Chem.*, 2012, **4**, 854–859.

48 I. Ghosh, T. Ghosh, J. I. Bardagi and B. König, Reduction of aryl halides by consecutive visible light-induced electron transfer processes, *Science*, 2014, **346**, 725–728.

49 P. Enders, M. Májek, C. M. Lam, R. D. Little and R. Francke, How to Harness Electrochemical Mediators for Photocatalysis - A Systematic Approach Using the Phenanthro[9,10-]imidazole Framework as a Test Case, *ChemCatChem*, 2023, **15**, e202200830.

50 I. A. MacKenzie, L. Wang, N. P. R. Onuska, O. F. Williams, K. Begam, A. M. Moran, B. D. Dunietz and D. A. Nicewicz, Discovery and characterization of an acridine radical photoreductant, *Nature*, 2020, **580**, 76–80.

51 S. Wu, T. H. Wong, P. Righi and P. Melchiorre, Photochemical Organocatalytic Synthesis of Thioethers from Aryl Chlorides and Alcohols, *J. Am. Chem. Soc.*, 2024, **146**, 2907–2912.

52 S. Wu, F. Schiel and P. Melchiorre, A General Light-Driven Organocatalytic Platform for the Activation of Inert Substrates, *Angew. Chem., Int. Ed.*, 2023, **62**, e202306364.

53 X. Q. Xie, W. Zhou, R. C. Yang, X. R. Song, M. J. Luo and Q. Xiao, Electroreduction strategy: a sustainable tool for the generation of aryl radicals, *Org. Chem. Front.*, 2024, **11**, 4318–4342.

54 H. Kim, H. Kim, T. H. Lambert and S. Lin, Reductive Electrophotocatalysis: Merging Electricity and Light To Achieve Extreme Reduction Potentials, *J. Am. Chem. Soc.*, 2020, **142**, 2087–2092.

55 N. G. W. Cowper, C. P. Chernowsky, O. P. Williams and Z. K. Wickens, Potent Reductants via Electron-Primed Photoredox Catalysis: Unlocking Aryl Chlorides for Radical Coupling, *J. Am. Chem. Soc.*, 2020, **142**, 2093–2099.

56 A. L. J. Beckwith, C. J. Easton and A. K. Serelis, Some guidelines for radical reactions, *J. Chem. Soc., Chem. Commun.*, 1980, 482–483, DOI: 10.1039/c39800000482.

57 F. Brandl, S. Bergwinkl, C. Allacher and B. Dick, Consecutive Photoinduced Electron Transfer (conPET): The Mechanism of the Photocatalyst Rhodamine 6G, *Chem. – Eur. J.*, 2020, **26**, 7946–7954.

58 J. D. Scott and R. M. Williams, Chemistry and biology of the tetrahydroisoquinoline antitumor antibiotics, *Chem. Rev.*, 2002, **102**, 1669–1730.

59 C. Li, R. Dickson, N. Rockstroh, J. Rabeah, D. B. Cordes, A. M. Z. Slawin, P. Hünemörder, A. Spannenberg, M. Bühl, E. Mejía, E. Zysman-Colman and P. C. J. Kamer, Ligand electronic fine-tuning and its repercussion on the photocatalytic activity and mechanistic pathways of the copper-photocatalysed aza-Henry reaction, *Catal. Sci. Technol.*, 2020, **10**, 7745–7756.

60 X. Guo, J. Rabeah, R. Sun, D. Wang and E. Mejía, Fluorescent Hybrid Porous Polymers as Sustainable Heterogeneous Photocatalysts for Cross-Dehydrogenative Coupling Reactions, *ACS Appl. Mater. Interfaces*, 2021, **13**, 42889–42897.

61 P. Enders, K. Prane, E. Schönke, T. Taeufer, D. Michalik, J. Rabeah and R. Francke, Cation Radical Newman-Kwart Rearrangement Enabled by Heterogeneous Photocatalysis under Mild Conditions, *ChemCatChem*, 2023, **15**, e202300744.

62 S. S. Zhu, Y. Liu, X. L. Chen, L. B. Qu and B. Yu, Polymerization-Enhanced Photocatalysis for the Functionalization of C(sp)-H Bonds, *ACS Catal.*, 2022, **12**, 126–134.

63 H. Bartling, A. Eisenhofer, B. König and R. M. Gschwind, The Photocatalyzed Aza-Henry Reaction of Aryltetrahydroisoquinolines: Comprehensive Mechanism, $H^{\bullet}$- versus H+-Abstraction, and Background Reactions, *J. Am. Chem. Soc.*, 2016, **138**, 11860–11871.

64 I. Saito, T. Matsuura and K. Inoue, Formation of Superoxide Ion Via One-Electron Transfer from Electron-Donors to Singlet Oxygen, *J. Am. Chem. Soc.*, 1983, **105**, 3200–3206.

65 W. H. Koppenol, D. M. Stanbury and P. L. Bounds, Electrode potentials of partially reduced oxygen species, from dioxygen to water, *Free Radical Biol. Med.*, 2010, **49**, 317–322.

66 J. L. Clement, N. Ferre, D. Siri, H. Karoui, A. Rockenbauer and P. Tordo, Assignment of the EPR spectrum of 5,5-dimethyl-1-pyrroline N-oxide (DMPO) superoxide spin adduct, *J. Org. Chem.*, 2005, **70**, 1198–1203.

67 M. C. DeRosa and R. J. Crutchley, Photosensitized singlet oxygen and its applications, *Coord. Chem. Rev.*, 2002, **233**, 351–371.

68 Y. Pan, S. Wang, C. W. Kee, E. Dubuisson, Y. Yang, K. P. Loh and C.-H. Tan, Graphene oxide and Rose Bengal: oxidative C–H functionalisation of tertiary amines using visible light, *Green Chem.*, 2011, **13**, 3341–3344.

69 Q. Wan, Y. Li, K. Ding, Y. Xie, J. Fan, J. Tong, Z. Zeng, Y. Li, C. Zhao, Z. Wang and B. Z. Tang, Aggregation Effect on Multiperformance Improvement in Aryl-Armed Phenazine-Based Emitters, *J. Am. Chem. Soc.*, 2023, **145**, 1607–1616.

70 S. E. Vaillard, C. Muck-Lichtenfeld, S. Grimme and A. Studer, Homolytic substitution at phosphorus for the synthesis of alkyl and aryl phosphanes, *Angew. Chem., Int. Ed.*, 2007, **46**, 6533–6536.

71 A. A. Folgueiras-Amador, A. E. Teuten, M. Salam-Perez, J. E. Pearce, G. Denuault, D. Pletcher, P. J. Parsons, D. C. Harrowven and R. C. D. Brown, Cathodic Radical Cyclisation of Aryl Halides Using a Strongly-Reducing Catalytic Mediator in Flow, *Angew. Chem., Int. Ed.*, 2022, **61**, e202203694.

72 C. Mudithanapelli, L. P. Dhorma and M. H. Kim, PIFA-Promoted, Solvent-Controlled Selective Functionalization of C(sp(2))-H or C(sp(3))-H: Nitration via C-N Bond Cleavage of CH(3)NO(2), Cyanation, or Oxygenation in Water, *Org. Lett.*, 2019, **21**, 3098–3102.

73 E. E. Bjerg, J. Marchan-Garcia, E. Buxaderas, Y. Moglie and G. Radivoy, Oxidative alpha-Functionalization of 1,2,3,4-Tetrahydroisoquinolines Catalyzed by a Magnetically Recoverable Copper Nanocatalyst. Application in the Aza-Henry Reaction and the Synthesis of 3,4-Dihydroisoquinolones, *J. Org. Chem.*, 2022, **87**, 13480–13493.

74 S. Zhang, L. Ma, W. Ma, L. Chen, K. Gao, S. Yu, M. Zhang, L. Zhang and G. He, Selenoviologen-Appendant Metallacycles with Highly Stable Radical Cations and Long-Lived Charge Separation States for Electrochromism and Photocatalysis, *Angew. Chem., Int. Ed.*, 2022, **61**, e202209054.

75 J. W. Zhou, S. P. Wang, Y. M. Lu, L. M. Li, W. T. Duan, Q. Wang, H. Wang and W. T. Wei, Solvent-driven C(sp3)-H thiocarbonylation of benzylamine derivatives under catalyst-free conditions, *Green Chem.*, 2021, **23**, 767–773.

76 Y. Katsurayama, Y. Ikabata, H. Maeda, M. Segi, H. Nakai and T. Furuyama, Direct Near Infrared Light-Activatable Phthalocyanine Catalysts, *Chem. – Eur. J.*, 2022, **28**, e202103223.

77 G. V. Morozkov, A. S. Abel, K. A. Lyssenko, V. A. Roznyatovsky, A. D. Averin, I. P. Beletskaya and A. Bessmertnykh-Lemeune, Ruthenium(II) complexes with phosphonate-substituted phenanthroline ligands as reusable photoredox catalysts, *Dalton Trans.*, 2024, **53**, 535–551.

78 Z. Chen, X. Chen and C. M. So, Palladium-Catalyzed C(sp(2))-N Bond Cross-Coupling with Triaryl Phosphates, *J. Org. Chem.*, 2019, **84**, 6366–6376.

79 B. Groll, P. Schaaf and M. Schnurch, Improved simplicity and practicability in copper-catalyzed alkynylation of tetrahydroisoquinoline, *Monatsh. Chem.*, 2017, **148**, 91–104.

80 V. Vinayagam, S. K. Sadhukhan, S. K. Karre, R. Srinath, R. K. Maroju, P. R. Karra, H. Bathula, S. Kundrapu and S. R. Surukonti, TBAT-Catalyzed Deoxygenative Reduction of Tertiary Amides to Amines, *Org. Lett.*, 2023, **25**, 4610–4614.

81 F. Xu, F. Zhang, W. Wang, M. Yao, X. Lin, F. Yang, Y. Qian and Z. Chen, Iron(III)-catalyzed alpha-cyanation and carbonylation with 2-pyridylacetonitrile: divergent synthesis of alpha-amino nitriles and tetrahydroisoquinolinones, *Org. Biomol. Chem.*, 2022, **20**, 7031–7035.

82 Q. W. Gui, Z. Y. Xiong, F. Teng, T. C. Cai, Q. Li, W. Hu, X. Wang, J. Yu and X. Liu, Electrochemically promoted oxidative alpha-cyanation of tertiary and secondary amines using cheap AIBN, *Org. Biomol. Chem.*, 2021, **19**, 8254–8258.

83 A. M. Nauth, N. Otto and T. Opatz, α-Cyanation of Aromatic Tertiary Amines using Ferricyanide as a Non-Toxic Cyanide Source, *Adv. Synth. Catal.*, 2015, **357**, 3424–3428.

84 Q. B. Liao, W. T. Xu, X. Huang, C. Ke, Q. Zhang, K. Xi and J. Xie, Donor-acceptor type [4+3] covalent organic frameworks: sub-stoichiometric synthesis and photocatalytic application, *Sci. China:Chem.*, 2020, **63**, 707–714.

85 Q. Xia, Y. Li, L. Cheng, X. Liang, C. Cao, P. Dai, H. Deng, W. Zhang and Q. Wang, Electron Donor-Acceptor Complex-Initiated Photochemical Cyanation for the Preparation of alpha-Amino Nitriles, *Org. Lett.*, 2020, **22**, 9638–9643.

86 Z. Fu, Y. Fu, J. Yin, G. Hao, X. Yi, T. Zhong, S. Guo and H. Cai, Electrochemical strategies for N-cyanation of secondary amines and α C-cyanation of tertiary amines under transition metal-free conditions, *Green Chem.*, 2021, **23**, 9422–9427.

87 M. Periasamy, M. Shanmugaraja, P. O. Reddy, M. Ramusagar and G. A. Rao, Synthetic Transformations Using Molecular Oxygen-Doped Carbon Materials, *J. Org. Chem.*, 2017, **82**, 4944–4948.

88 T. Q. Ye, Y. Z. Li, Y. N. Ma, S. P. Tan and F. Li, Aerobic Benzylic C(sp3)-H Bond Oxygenations Catalyzed by NBS under Visible Light Irradiation, *J. Org. Chem.*, 2023, **89**, 534–540.

89 V. V. Pavlishchuk and A. W. Addison, Conversion constants for redox potentials measured versus different reference electrodes in acetonitrile solutions at 25 °C, *Inorg. Chim. Acta*, 2000, **298**, 97–102.

90 L. Buzzetti, G. E. M. Crisenza and P. Melchiorre, Mechanistic Studies in Photocatalysis, *Angew. Chem., Int. Ed.*, 2019, **58**, 3730–3747.

91 W.-L. Jiang, B. Huang, X.-L. Zhao, X. Shi and H.-B. Yang, Strong halide anion binding within the cavity of a conformation-adaptive phenazine-based Pd2L4 cage, *Chem*, 2023, **9**, 2655–2668.

92 (*a*) CCDC 2379436: Experimental Crystal Structure Determination, 2025, DOI: **10.5517/ccdc.csd.cc2kw00h**; (*b*) CCDC 2432793: Experimental Crystal Structure Determination, 2025, DOI: **10.5517/ccdc.csd.cc2mnj61**.